

Earth's Future

RESEARCH ARTICLE

10.1029/2024EF005021

Limited Effect of Future Land-Use Changes on Human Heat Stress and Labor Capacity



Key Points:

- Land use change effects on heat stress and temperature are different due to counteracting biogeophysical effects on humidity and wind speed
- In a low-emission scenario, the climate effect of future land-use change can determine if the global temperature targets will be achieved
- The land use change effects on heat stress and labor capacity are uncertain across ESMs and small compared to the effects of climate change

Correspondence to:

S. J. De Hertog,
Steven.DeHertog@UGent.be






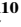






Citation:

De Hertog, S. J., Orlov, A., Havermann, F., Guo, S., Manola, I., Pongratz, J., et al. (2025). Limited effect of future land-use changes on human heat stress and labor capacity. *Earth's Future*, 13, e2024EF005021. <https://doi.org/10.1029/2024EF005021>

Received 19 JUN 2024
Accepted 29 NOV 2024

Author Contributions:

Conceptualization: Steven J. De Hertog, Anton Orlov, Wim Thiery
Formal analysis: Steven J. De Hertog, Anton Orlov
Funding acquisition: Julia Pongratz, Quentin Lejeune, Carl-Friedrich Schleussner, Inga Menke, Florian Humpenöder, Alexander Popp, Wim Thiery
Methodology: Steven J. De Hertog, Felix Havermann, Suqi Guo, Iris Manola, Peter Lawrence, George C. Hurtt, Louise Chini, Inne Vanderkelen, Thomas Reerink
Supervision: Wim Thiery
Writing – original draft: Steven J. De Hertog, Anton Orlov
Writing – review & editing: Steven J. De Hertog, Anton Orlov, Felix Havermann, Suqi Guo, Iris Manola, Julia Pongratz, Quentin Lejeune, Carl-Friedrich Schleussner, Inga Menke,

Steven J. De Hertog^{1,2} , Anton Orlov³ , Felix Havermann⁴, Suqi Guo⁴, Iris Manola⁵, Julia Pongratz^{4,6}, Quentin Lejeune⁷, Carl-Friedrich Schleussner⁷ , Inga Menke⁷, Florian Humpenöder⁸ , Alexander Popp⁸, Peter Lawrence⁹ , George C. Hurtt¹⁰ , Louise Chini¹⁰ , Inne Vanderkelen^{11,12,13} , Edouard L. Davin^{11,12,13}, Thomas Reerink¹⁴ , Sonia I. Seneviratne¹⁵ , Hans Verbeek² , and Wim Thiery¹ 

¹Department of Water and Climate, Vrije Universiteit Brussel, Brussels, Belgium, ²Q-ForestLab, Department of Environment, Universiteit Gent, Ghent, Belgium, ³Centre for International Climate Research, Oslo, Norway, ⁴Department of Geography, Ludwig-Maximilians-Universität in Munich, Munich, Germany, ⁵Vrije Universiteit Amsterdam, Institute for Environmental Studies, Amsterdam, The Netherlands, ⁶Max Planck Institute for Meteorology, Hamburg, Germany, ⁷Climate Analytics, Berlin, Germany, ⁸Potsdam Institute for Climate Impact Research, Potsdam, Germany, ⁹National Centre for Atmospheric Research, Boulder, CO, USA, ¹⁰Department of Geographical Sciences, University of Maryland, College Park, MD, USA, ¹¹Wyss Academy for Nature at the University of Bern, Bern, Switzerland, ¹²Climate and Environmental Physics Division, University of Bern, Bern, Switzerland, ¹³Oeschger Centre for Climate Change Research, University of Bern, Bern, Switzerland, ¹⁴Royal Netherlands Meteorological Institute (KNMI), De Bilt, The Netherlands, ¹⁵ETH Zurich, Institute for Atmospheric and Climate Science, Zurich, Switzerland

Abstract To achieve the 1.5°C target of the Paris agreement, rapid, sustained, and deep emission reductions are required, which often includes negative emissions through land-based mitigation. However, the effects of future land-use change on climate are often not considered when quantifying the climate-induced impacts on human heat stress and labor capacity. By conducting simulations with three fully coupled Earth System Models, we project the effects of land-use change on heat stress and outdoor labor capacity for two contrasting future land-use scenarios under high-ambition mitigation. Achieving a sustainable land-use scenario with increasing global forest cover instead of an inequality scenario with decreasing forest cover in the Global South causes a global cooling ranging between 0.09°C and 0.35°C across the Earth System Models. However, the effects on human heat stress are less strong, especially over the regions of intense land-use change such as the tropics, where biogeophysical effects on near-surface specific humidity and wind speed counteract the cooling effect under warm extremes. The corresponding influence on outdoor labor capacity is small and inconsistent across the three Earth System Models. These results clearly highlight the importance of land-use change scenarios for achieving global temperature targets while questioning the adaptation potential for reduction in heat stress.

Plain Language Summary Land transformations play a significant role in Paris-Agreement-compatible pathways that limit global warming to 1.5°C or 2°C. Besides altering carbon uptake and release, land-use changes also influence the climate by modifying the amount of evaporation, the reflection of sunlight, and other surface properties. Earth System Models currently disagree between each other about these effects. Here we apply three climate models to investigate the effects of two different land-use scenarios representing alternative future societies: (a) a sustainability scenario where tropical forests are preserved and afforestation is implemented and (b) an inequality scenario with large-scale tropical deforestation. We find that the sustainability scenario results in more land-use-induced cooling compared to the inequality scenario, in addition to higher land carbon storage. In contrast, Land-use changes affect heat stress in a complex way, with deforestation overall leading to a decreased heat stress in the tropics. These effects are however less clear during extreme conditions and appear to affect labor capacity over those regions in a limited way. This implies that the potential of forestation for limiting heat stress impacts of climate change is limited.

1. Introduction

Land-use changes (LUC) are expected to play a major role toward the future, as most socio-economic scenarios in line with the Paris Agreement require large-scale carbon dioxide removals (Pongratz et al., 2021; Roe et al., 2019). Land-based mitigation, such as enhanced carbon sequestration through afforestation and bio-energy plantations with carbon capture and storage (IPCC, 2022; Roe et al., 2019; Rogelj et al., 2018), will be

© 2025. The Author(s).

This is an open access article under the terms of the [Creative Commons Attribution License](https://creativecommons.org/licenses/by/4.0/), which permits use, distribution and reproduction in any medium, provided the original work is properly cited.

Florian Humpenöder, Alexander Popp,
Peter Lawrence, George C. Hurtt,
Louise Chini, Inne Vanderkelen, Edouard
L. Davin, Thomas Reerink, Sonia
I. Seneviratne, Hans Verbeeck,
Wim Thiery

required in addition to rapid, sustained, and deep fossil fuel emission reductions, to ensure that the world does not pass the Paris agreement target of 1.5°C increase in global mean temperature (IPCC, 2021, 2022; Rogelj et al., 2018; UNFCCC, 2015). However, the effects of the associated future LUC on the climate remain poorly understood (Pongratz et al., 2021).

Future socio-economic scenarios typically only consider LUC-induced effects through changes in the carbon cycle (biogeochemical effects), but neglect the effects on surface properties which change the surface energy and water cycles (biogeophysical effects) (Pongratz et al., 2021). The biogeophysical effects have been shown to be substantial regionally but remain uncertain within different Earth System Models (ESM), and frequently even disagree on the sign of change (Boysen et al., 2020; De Hertog et al., 2023). It is crucial to better understand the effects of LUC on the climate, in order to properly inform the current and near-future climate policy (Duveiller et al., 2020; Pongratz et al., 2021). ESM simulations dedicated to assess the LUC-induced effects on climate generally focus on historical (Boisier et al., 2012; De Noblet-Ducoudré et al., 2012; Pitman et al., 2009; Pongratz et al., 2010) or highly idealized simulation setups (Boysen et al., 2020; Davin & de Noblet-Ducoudre, 2010; De Hertog et al., 2023; Portmann et al., 2022; Winckler et al., 2017, 2019), with only few simulations explicitly assessing LUC-induced climate effects under future scenarios (Boysen et al., 2014; Brovkin et al., 2013; Hirsch et al., 2018). However, as many of the relevant biogeophysical and biogeochemical processes depend on the background climate (Pongratz et al., 2021), the entire ecosystem-climate feedback needs to be considered. This can be achieved by conducting dedicated future emission-driven simulations that more accurately quantify the LUC-induced climate effects of low-warming scenarios that heavily rely on land-based climate change mitigation.

LUC-induced climate effects have been shown to play an even larger role during heat extremes. For example, historical deforestation caused more extreme heat in the Northern mid-latitudes (Lejeune et al., 2018), while afforestation over Europe has been shown to increase summer precipitation (Meier et al., 2021). This illustrates that LUC could, besides from their mitigation potential, also modulate and thus potentially play a role in adapting to the impacts of future climate change (Davin et al., 2014; Pongratz et al., 2021; Seneviratne et al., 2018). However, studies assessing the adaptation potential of LUC are typically limited to single meteorological variables such as temperature, which makes it unclear how these translate to direct impacts on human beings through heat stress (Orlov, De Hertog et al., 2023). In addition to temperature, LUC also affect near-surface relative humidity, wind speed and incoming surface shortwave radiation which determine the impact on heat stress (Orlov, De Hertog et al., 2023). Future heat stress is important for health but also affects the economy through a reduction in working hours (labor capacity) due to, for example, climate-induced injuries (Fatima et al., 2021). Heat-induced reductions in labor capacity can be substantial especially over low-latitude regions, which are typically regions where adaptive capacity is low (Kjellstrom et al., 2018; Mora et al., 2017). While labor capacity will be substantially afflicted as a result of future greenhouse gas emissions (Orlov et al., 2020; Orlov, Jägermeyr, et al., 2024), it is currently unclear how this will be affected by future LUC scenarios.

Here we aim to disentangle the LUC-induced climate effects on heat stress and labor capacity under a future low warming scenario. To achieve this, we perform and analyze a set of dedicated ESM projections that incorporate two recently developed LUC scenarios. These scenarios represent two different global future socio-economic contexts: (a) a global narrative of non-converging socio-economic conditions, which leads to measures to maintain sustainable land use being only implemented in high-income countries (inequality scenario), versus (b) a narrative of converging socio-economic conditions that support global measures such as greenhouse gas emission pricing, sustainable land-use practices, and inclusive socio-economic development (sustainability scenario) (Humpenöder et al., 2022). The simulations are set up under an emission-driven, well below 2°C compatible scenario to assess the importance of LUC-induced climate effects on human heat stress and labor capacity in a low-warming future. First, we analyze these results for the effects on global and regional mean temperature. Next, we assess the impacts of these LUC-induced temperature changes by quantifying LUC-induced effects on humid heat stress and consequent changes in labor capacity.

2. Methods

2.1. Participating ESMs

This study is conducted using three state-of-the-art ESMs: the Community Earth System Model (CESM), the Max Planck Institute for Meteorology Earth System Model (MPI-ESM), and the European Consortium Earth System Model (EC-EARTH). Here, we provide a brief technical description of each model.

We apply CESM version 2.1.3, which is a community built open source ESM (Danabasoglu et al., 2020). The model is run in fully coupled mode at $0.90^\circ \times 1.25^\circ$ spatial resolution. The ESM includes an atmosphere model (the Community Atmosphere Model version 6; CAM6), a land model (the Community Land Model version 5; CLM5), an ocean model (the Parallel Ocean Program version 2; POP2), an ice sheet model (the Community Ice Sheet Model; CISM), and a sea ice model (the Los Alamos National Laboratory Sea Ice model, CICE).

We use the Max Planck Institute for Meteorology Earth System Model version 1.2 with low resolution configuration (MPI-ESM1.2-LR) at $1.88^\circ \times 1.88^\circ$ spatial resolution (Mauritsen et al., 2019). The MPI-ESM uses ECHAM6.3 as the atmosphere model, JSBACH3.2 as the land surface model, and a coupled ocean dynamics and biogeochemistry model (MPIOM1.6 and HAMOCC6, respectively).

The European Consortium Earth System Model version 3 (EC-EARTH-CC) is a state-of-the-art Earth system model developed by the EC-Earth consortium (Döscher et al., 2022). The model is run in fully coupled mode at a $0.7^\circ \times 0.7^\circ$ spatial resolution. It uses the Integrated Forecast System (IFS) as an atmosphere model, which includes a component to handle surface and water energy exchanges from the surface: the Hydrology Tiled ECMWF Scheme for Surface Exchanges over Land (HTESSEL). HTESSEL couples the atmosphere model to the land model: Lund-Potsdam-Jena General Ecosystem Simulator (LPJ-GUESS). The oceanic component is modeled through the Nucleus for European Modeling of the Ocean (NEMO) model (v3.6) and the Pelagic Interactions Scheme for Carbon and Ecosystem Studies volume 2 (PISCES) that models the oceanic biogeochemistry.

These ESMs have participated in several multi-model intercomparison projects focusing on the effects of LUC on the climate (e.g., LUMIP, Boysen et al., 2020). Each of the ESMs have been evaluated for their capacity to model LUC-induced temperature effects (De Hertog et al., 2023) and have been shown to perform reasonably well for LUC-induced changes in annual mean surface temperature.

2.2. Simulation Setup

We conduct four simulations for every ESM: one for the present-day and three future simulations (Figure 1). For the present-day simulations, we conduct a short 35-year simulation (presCTL; 1980–2014) which branches off in 1980 from the first three members of the *esm-hist* simulations, performed with the respective ESMs within the context of the Coupled Model Intercomparison Project Phase 6 (CMIP6) (Eyring et al., 2016). Thus, each of the three ESMs produced an ensemble of three present-day simulations. For CESM, only two members of *esm-hist* were available, hence the third ensemble member was generated through a slight initial condition perturbation in the atmospheric temperature field of the first member for this ESM. The future climate (2015–2100, futCTL) is simulated by branching off from the three presCTL simulations per ESM. We first perform a simulation of the future climate (2015–2100) under a low-warming scenario (RCPI.9) without LUC. In both the futCTL and presCTL ensemble, the land use is kept constant at present-day levels (representing the end of 2014 conditions). Next to the futCTL, two additional experiments with transient LUC are conducted under RCPI.9 forcing, with details provided below.

All ESMs run in an emission-driven mode, meaning that atmospheric CO_2 concentration is a prognostic variable during the runtime of the simulation. In emission-driven mode, the atmospheric CO_2 concentration is computed from anthropogenic fossil and industrial emissions as well as from terrestrial and ocean C exchange. This CO_2 concentration change in the atmosphere then affects the energy and water cycle (biogeophysical effects) which in turn alters the terrestrial and ocean C exchange (biogeochemical effects) with a feedback to atmospheric CO_2 concentrations. In our study, the applied LUC scenarios additionally affect terrestrial C exchange, which in turn alters the atmospheric CO_2 concentration and thus adds to the overall feedback mechanisms of the Earth System.

The future LUC scenarios driving the two simulations with transient land use are derived from the agro-economic land-use model MAGPIE (Model of Agricultural Production and its Impact on the Environment) and were first presented in Humpenöder et al. (2022). They represent two starkly different futures with regard to socio-economic development, environmental protection, and land-based mitigation. In the sustainability scenario (SUST), the world undergoes a transition in which mitigation in the Agriculture, Forestry and Other Land Use (AFOLU) sector is strongly incentivized via carbon pricing mechanisms and generalized environmental protection measures. Moreover, socio-economic development is assumed to follow an even more sustainable trajectory than in the SSP1 scenario (Soergel et al., 2021), resulting in less pressure on land ecosystems due to

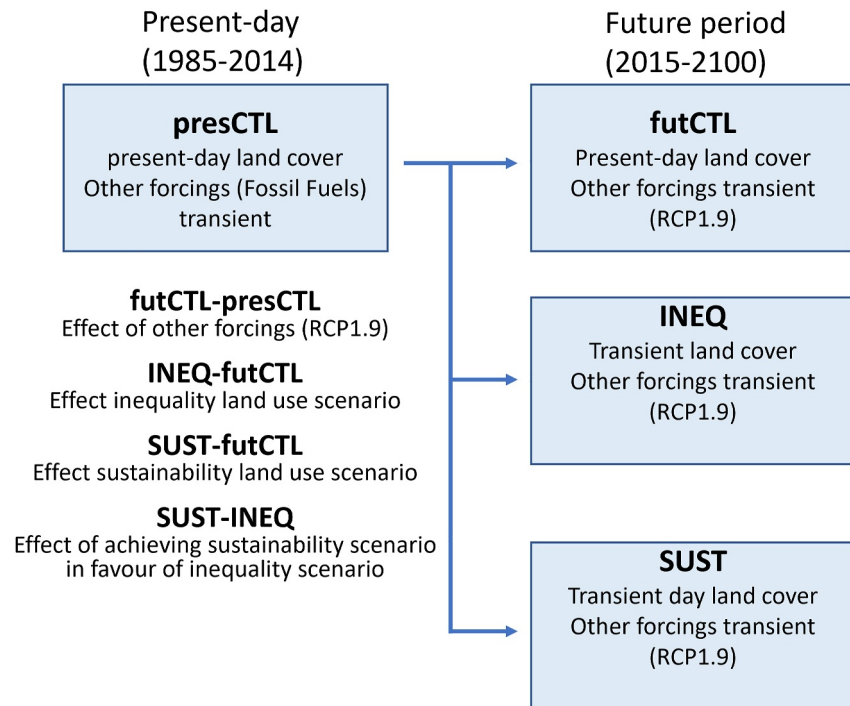


Figure 1. Schematic highlighting the simulation setup: Two control simulations, one for a present-day period (1985–2014; presCTL) and one for a future period (2015–2100; futCTL) using RCP1.9 forcing. For both control simulations, land use is kept constant at the 2014 levels. The two additional future simulations are performed using land-use scenarios from Humpenöder et al. (2022), one representing land use following the inequality scenario (INEQ) and the other representing land use following the sustainability scenario (SUST).

reduced demand for land-based products (Riahi et al., 2017). In contrast, the Inequality scenario (INEQ) follows the narrative of the SSP4 scenario (Riahi et al., 2017). In this scenario, the developments characterizing SUST are also observed in countries part of the Organisation for Economic Cooperation and Development (OECD), while the rest of world undergoes a continuation of current socio-economic trends and no additional carbon pricing or environmental protection measures are implemented (Humpenöder et al., 2022). For a full description of these land-use scenarios we refer to Humpenöder et al. (2022).

These land-use scenarios, derived with MAgPie, are implemented in the ESMs following the same procedure used in CMIP6 by harmonizing them with historical land-use reconstructions using the Land Use Harmonization 2 (LUH2) (Hurt et al., 2020) methodology. In addition, LUH2 provides a consistent data format for use in ESMs comprising 12 different land-use types, computes all transitions between land-use types (including wood harvest and shifting cultivation), provides area, age, and biomass of secondary land, and also provides land management data layers including irrigation, synthetic nitrogen fertilizer usage, and areas of afforestation (planted trees). For this project the LUH2 methodology was expanded to also include three different categories of protected land areas (on primary forest, secondary forest, and non-forest) that were excluded from agricultural expansion and wood harvesting. Secondly, we apply an ESM-specific translation scheme to translate the LUH2 land-use categories into native land-use maps and related Plant Functional Type definitions for each ESM (Lawrence et al., 2016). The LUH2 LUC for the INEQ and SUST scenarios by the end of the century are shown in Figure 2. The implementation of these LUH2 land-use patterns within the MPI-ESM and CESM is shown in Appendix A while EC-EARTH uses the LUH2 data directly as an input. In the sustainability scenario, there is a general decrease in cropland due to population changes and dietary changes. These abandoned croplands are then often afforested, such as across the US, while there is also afforestation occurring at the expense of grasslands. In the Inequality scenario, there is a strong increase in cropland area at the expense of previously forested and grassland areas, especially in the tropics. In Europe and North America, there is some afforestation even in this scenario. These different socioeconomic scenarios lead to clearly different LUC throughout the future period, especially over the tropics.

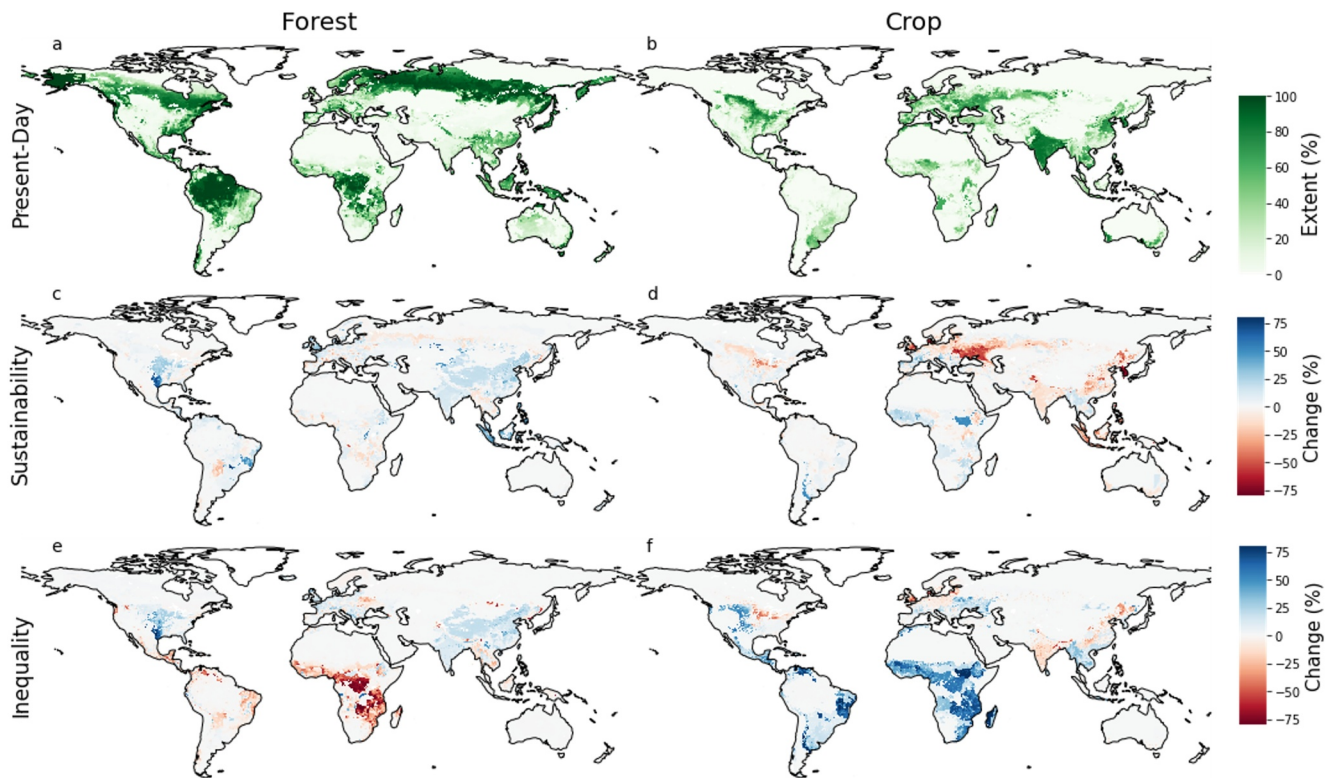


Figure 2. Land-use patterns showing the amount of forest (a) and cropland (b) as a grid cell fraction (%) within the CTL simulations (2014 land-use extent). The change for the sustainability (c, d) and inequality scenarios (e, f) are shown for forest (c, e) and cropland (d, f) by the end of the century.

Within the ESMs used here, only CESM includes irrigation-induced effects on the climate (Thiery et al., 2017, 2020; Yao et al., 2022). In CESM, the different scenarios thus also affect irrigation extent (see Appendix B). In EC-EARTH, irrigation is modeled within the land surface component but is not coupled to the atmosphere and therefore has limited effects on the climate, even in extreme irrigation scenarios (De Hertog et al., 2023). Irrigation is not implemented in the default model version of MPI-ESM used here. To summarize, in both EC-EARTH and MPI-ESM the LUC scenarios only affect land cover changes, while in CESM, changes in irrigation extent are included within the different scenarios and cause biogeochemical and biogeophysical effects on climate.

The simulation setup (Figure 1) enables the analysis of the climate effects between the two alternative future scenarios (SUST-INEQ) as well as the climate effects of the sustainability land-use scenario (SUST-futCTL) and the inequality land-use scenario (INEQ-futCTL) individually. In addition, the climate effects as a response to RCP1.9 forcing in absence of any LUC (futCTL-presCTL) can also be derived and is used as a benchmark for the importance for the LUC-induced climate effects. Three ensemble members are run for each of the experiments to smooth out the effect of internal variability. All climatological variables are analyzed as averages over 30-year time slices (1985–2014 for presCTL, 2070–2099 for future experiments) and are tested for statistical significance (Sig.) using a two-sided Wilcoxon signed rank test of lumped ensemble members at the 0.05 significance level (Wilks, 2006). Additionally, for the spatial maps, we test for field significance using the false discovery rate to take spatial autocorrelations into account (Lorenz et al., 2016; Vanderkelen et al., 2021).

The version of CESM used in this study (CESM2.1.3) has, prior to this study, never been run under RCP1.9 forcings. This implies that under the default configuration of CESM (using the Community Atmosphere Model as the atmosphere component), certain atmospheric forcings are not available for the RCP1.9 scenario, as these are generally derived from computationally more expensive simulations using the Whole Atmosphere Community Climate Model (WACCM) (Danabasoglu et al., 2020). The fields which are generally defined from these more complex runs include nitrogen deposition on land and the ocean surface as well as stratospheric ozone, aerosols,

methane oxidation and, tropospheric oxidants. To remain as consistent as possible to the RCP1.9 forcing, we apply these non-greenhouse gas forcing fields from the nearest scenario available (RCP2.6) in CESM.

2.3. Quantification of Heat Stress

Heat stress is determined by several climatic variables including temperature, relative humidity, incoming surface shortwave radiation and wind speed. Several diagnostic indices have been proposed to calculate heat stress based on climate variables (J. Buzan et al., 2015; Lemke & Kjellstrom, 2012). These approaches are often limited to empirical fittings of meteorological variables and can therefore be biased and often neglect important processes, such as the effects of incoming surface shortwave radiation or wind speed (J. R. Buzan & Huber, 2020). Wet Bulb Globe Temperature (WBGT) is a physically based diagnostic of heat stress that takes these processes into account by using the principles of heat and mass transfer (Yaglou & Minard, 1957; Liljegren et al., 2008; J. R. Buzan & Huber, 2020). The WBGT is an ISO standard metric and is widely used for quantifying heat stress in the health literature (Budd, 2008; Liljegren et al., 2008; J. R. Buzan & Huber, 2020). In a recent systematic review covering the 230 known heat stress metrics (Ioannou, Mantzios, et al., 2022), the WBGT was found to be the most suitable indicator for assessing the effects of occupational heat stress (Ioannou, Tsoutsoubi, et al., 2022). Here we apply the WBGT using the approach presented in Liljegren et al. (2008). WBGT is computed from three temperatures; dry bulb (ambient) temperature (T_a), natural wet-bulb temperature (T_w), which is the temperature that a freely evaporating surface is able to approach (e.g., sweaty skin), and black globe temperature (T_g), which is a metric for radiant heat of the environment, including direct sunlight, infrared radiation, and the temperature of surrounding objects.

$$WBGT = 0.7T_w + 0.2T_g + 0.1T_a \quad (1)$$

Where T_a is directly available from the ESM output, T_w and T_g need to be calculated in postprocessing. The equations of T_w and T_g need to be solved iteratively (Liljegren et al., 2008). We compute these values and the resulting WBGT using the recent python implementation of Liljegren's model by Kong and Huber (2022).

As these equations require an iterative solution it becomes computationally highly expensive to calculate WBGT for large climate data sets. Therefore, several previous studies have relied on derivative metrics such as simplified wet bulb globe temperature (sWBGT) and Environmental Stress Index (ESI) as a substitute for WBGT. A recent study found that ESI performs reasonably well as a substitute for WBGT, especially for assessing annual and seasonal mean effects on heat stress (Kong & Huber, 2022). However, a systematic review on occupational heat stress found that ESI was among the least performing metrics (Ioannou, Tsoutsoubi, et al., 2022). Despite this ESI and other simplified approximations remain used in scientific studies analyzing heat stress impacts on labor capacity (e.g., Orlov, De Hertog et al. (2023); Kamal et al. (2024)).

Several recent studies have found formulations of WBGT that are physically based and do not require an iterative solution (e.g., Brimicombe et al. (2022)). However, a recent study found that these alternative formulations still have some biases compared to the iterative solution (Kong & Huber, 2024b). For the analysis in this study, we focus on the iteratively computed WBGT but also quantify ESI (see Appendix F) and assess the validity of this empirical substitute for heat stress. The equation of ESI is provided below:

$$ESI = 0.63 * T_a - 0.03 * RH + 0.002 * S_{down} + 0.0054 * T_a * RH - \frac{0.073}{0.1 + S_{down}} \quad (2)$$

Where RH is relative humidity in %. All computations were performed using 3-hourly ESM output data to account for diurnal variations in the input variables.

2.4. Labor Capacity

To quantify the effects on labor capacity, defined as the occupational capacity to safely perform work under heat stress (Dunne et al., 2013), we apply the Physical Work Capacity Model presented in Havenith et al. (2024). The physical work capacity function was estimated through laboratory experiments simulating treadmill-regulated workloads, involving 982 participants. These experiments were conducted under varying conditions, including air temperature, humidity, wind speed, solar radiation, and types of clothing. The loss of physical work capacity

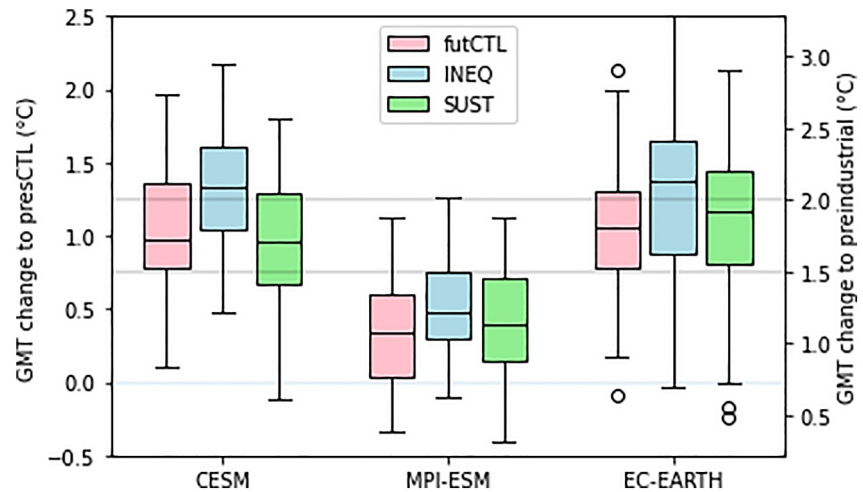


Figure 3. Boxplots representing the changes in Global Mean Temperatures (GMT) in °C within the CESM, MPI-ESM and EC-EARTH simulations for monthly data for the three ensemble members for futCTL, Inequality and Sustainability scenarios by the end of the century (2069–2099). The left axis highlights the GMT changes compared to the mean GMT in the presCTL period (1985–2015), while the right axis highlights those against the pre-industrial GMT (1850–1900) taken from HadCRUT5 (Morice et al., 2021). The gray lines indicate the Paris Agreement thresholds of 1.5°C and 2°C.

was measured as the total energy generated during hot trials compared to cool conditions. For the complete description of the model we refer to Havenith et al. (2024).

The labor capacity then is quantified as the percentage of a work hour that the worker is able to perform. We focus on high intensity jobs which are generally performed outside in the sun (such as construction and agriculture). We apply the calculation based on the “low clothing” model presented in Havenith et al. (2024) to represent an upper boundary of the effects of the meteorological conditions on workers.

To ensure intercomparability with previous studies, among which a study analyzing effects of idealized land cover change simulations using the same three ESMs (Orlov, De Hertog et al., 2023), we also quantify the often used metric based on the National Institute for Occupational Safety and Health (NIOSH) standards (Kjellstrom et al., 2009; NIOSH, 1986). These standards describe the frequency and duration of breaks from work required to avoid heat-induced illnesses. Here we use the limits recommended for a “standard” acclimatized worker of 70 kg. The values of labor capacity based on this approach are added in appendix G.

The effects on labor capacity for each method are computed from the WBGT metric at a 3-hourly temporal resolution. The 3-hourly heat stress values are first linearly interpolated to hourly data and converted to local time, then the effect on labor capacity is considered as the mean over a 12hr work day which is taken from 7 a.m. to 7 p.m.

3. Results

3.1. Climate Effects of Land-Use Scenarios

The effect of the very aggressive mitigation scenario (RCP1.9) without any LUC (futCTL-presCTL) causes a clear global warming in all three ESMs by the end of the century. However, the magnitude of this warming is less consistent across the ESMs (Figure 3). CESM is the warmest model with an increase in Global Mean Temperature (GMT) of 1.05°C [statistically significant at 95% (sig.), Confidence Interval (CI): 1.02 to 1.08] relative to presCTL (1.83°C compared to pre-industrial era 1850–1900), EC-EARTH shows a warming of 1.02°C [sig., CI: 0.99 to 1.05] (1.80°C compared to pre-industrial era), and MPI-ESM shows the lowest warming of only 0.35°C [sig., CI: 0.33 to 0.38] by the end of the century (1.13°C compared to the pre-industrial era). In MPI-ESM the GMT does not exceed the Paris Agreement target of 1.5°C global warming compared to pre-industrial era, while it is exceeded in both EC-EARTH and CESM in their futCTL ensembles. The warming shown for CESM and EC-EARTH is relatively high for a RCP 1.9 scenario. This is related to both being relatively “warm” models due to their high equilibrium climate sensitivity (i.e., the equilibrium amount of warming after a doubling of CO₂).

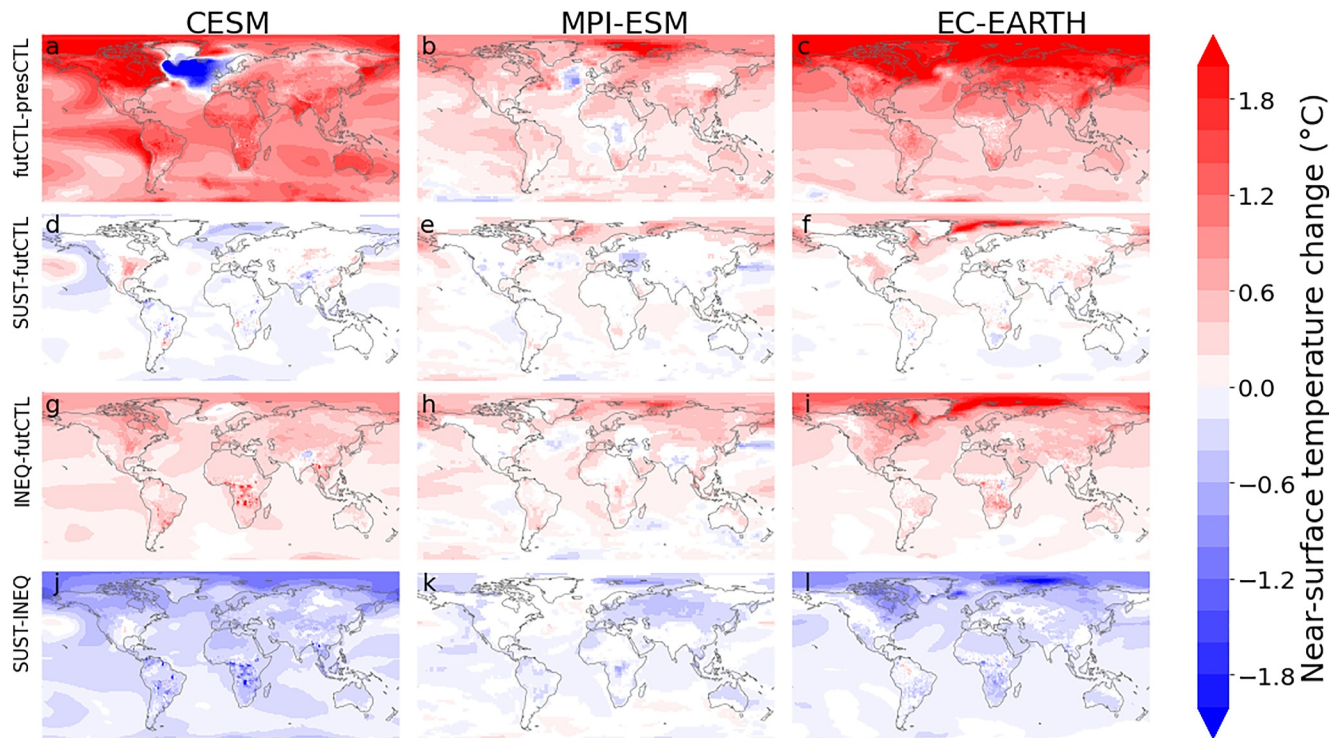


Figure 4. Changes in annual mean near-surface temperature (°C) by the end of the century (2070–2099) between the futCTL and presCTL scenarios, the sustainability and futCTL scenarios, the inequality and futCTL scenarios, and the sustainability and inequality scenarios, for CESM (a, d, g, j), MPI-ESM (b, e, h, k) and EC-EARTH (c, f, i, l), respectively. Only statistically significant changes are shown (0.05 significance level, two-sided Wilcoxon signed rank test of lumped ensemble members and field significance using the false discovery rate test).

of 5.2°C for CESM (Gettelman et al., 2019) and 4.3°C for EC-EARTH (Wyser et al., 2020) which both fall outside of the best estimate range of 2.5–4.0°C (Arias et al., 2021). The high climate sensitivity in this CESM version is largely caused by changes in cloud feedbacks over the tropical and Southern oceans (Bacmeister et al., 2020; Meehl et al., 2020), while in EC-EARTH it appears that the improved representation of aerosols, affecting cloud micro-physics would be the main cause (Meehl et al., 2020; Wyser et al., 2020). MPI-ESM, in contrast, has been tuned to a lower equilibrium climate sensitivity of 3°C in order to better match observations (Mauritsen & Roeckner, 2020).

The different LUC scenarios have a noticeable impact on GMT (Figure 3). The inequality scenario (INEQ-futCTL) consistently shows an additional warming across all ESMs, with CESM showing a warming of 0.29°C [sig., CI:0.27 to 0.31], EC-EARTH of 0.30°C [sig., CI:0.27 to 0.32] and MPI-ESM a warming of 0.17°C [sig., CI:0.15 to 0.19]. In both CESM and EC-EARTH, the 2°C global warming level is exceeded by the end of the century under the inequality scenario. The sustainability scenario (SUST-futCTL), in contrast, shows a slight cooling for CESM of -0.07°C [sig., CI:-0.04 to -0.09] and a slight warming of 0.05°C [sig., CI:0.04 to 0.08] in EC-EARTH and 0.06°C [sig., CI:0.04 to 0.09] in MPI-ESM.

These patterns in GMT can be further interpreted by analyzing the maps of near-surface air temperature by the end of the century (Figure 4). The RCP1.9 scenario (futCTL-presCTL) is causing a warming globally except for the North Atlantic Ocean in CESM and MPI-ESM, as well as over Central Africa in MPI-ESM where a cooling occurs (Figures 4a–4c). The North Atlantic cooling is a well-known feature within CESM where several simulations with moderate warming amounts show strong changes in Atlantic Meridional Overturning Circulation (AMOC) strength (Boysen et al., 2020; De Hertog et al., 2023; Portmann et al., 2022).

The sustainability scenario in CESM shows a slight global cooling effect except for some regions (e.g., Eastern USA) which show a warming (Figure 4d). In contrast, MPI-ESM and EC-EARTH (Figures 4e and 4f) show no clear global pattern with some regions showing a cooling (e.g., Central Europe in MPI-ESM) and some a warming (e.g., Eastern USA in EC-EARTH). The inequality scenario, in contrast, is causing a consistent

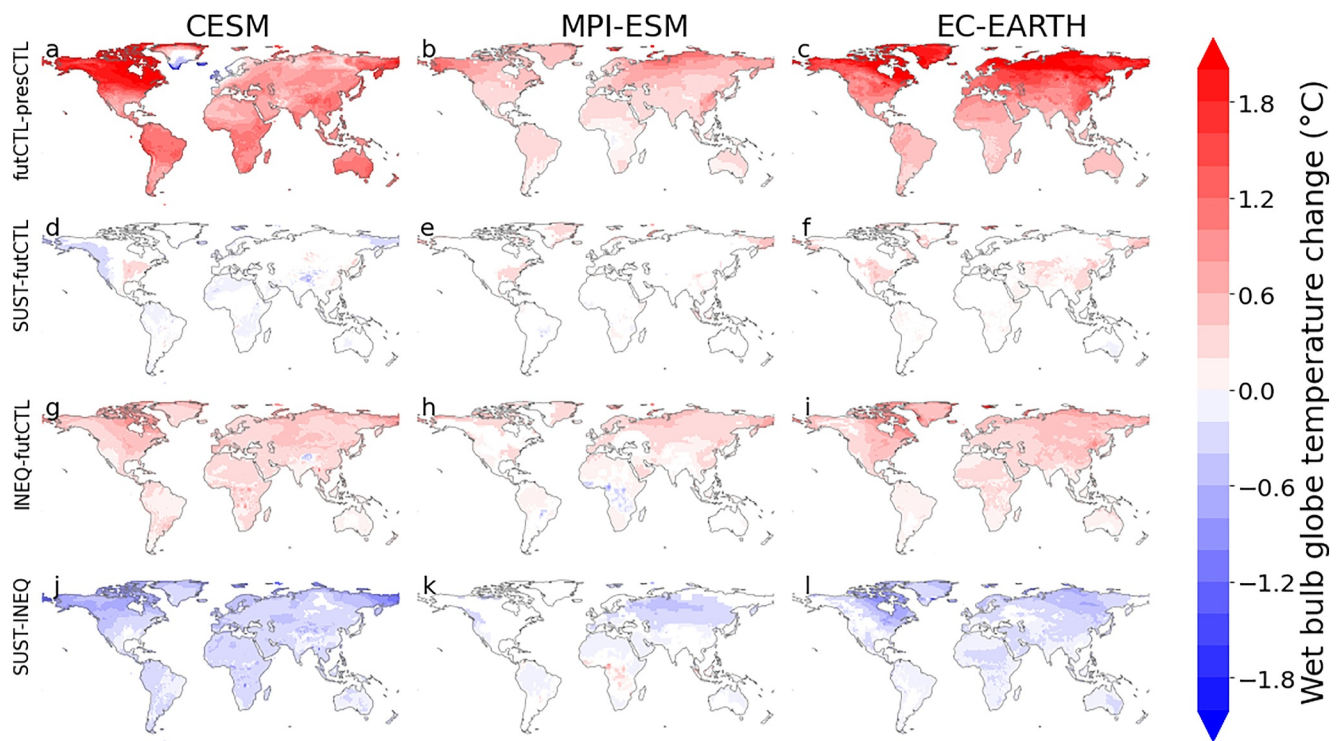


Figure 5. Changes in annual mean wet bulb globe temperature ($^{\circ}\text{C}$) by the end of the century (2070–2099) between the futCTL and presCTL scenarios, the sustainability and futCTL scenarios, the inequality and futCTL scenarios, and the sustainability and inequality scenarios, for CESM (a, d, g, j), MPI-ESM (b, e, h, k) and EC-EARTH (c, f, i, l), respectively. Only statistically significant changes are shown (0.05 significance level, two-sided Wilcoxon signed rank test of lumped ensemble members and field significance using the false discovery rate test).

temperature increase across all ESMs (Figures 4g, 4h, and 4i). However, for all three ESMs there is an enhanced warming over areas of intensive land use change such as Central Africa which goes up to local warming of 3°C in CESM. These global effects are likely a consequence of the increased LUC emissions as a consequence of the large-scale deforestation in this scenario (biogeochemical effect). While the temperature increase over areas of intensive LUC are likely dominated by local biogeophysical effects. The local biogeophysical effects have been analyzed for these three ESMs in a previous study (De Hertog et al., 2023). Deforestation was shown to cause warming over the tropics (as clearly apparent here over Central Africa in CESM). Over the northern hemisphere high latitudes, afforestation caused a warming, which is consistent with the results shown here.

Avoiding the inequality land-use scenario in favor of a sustainability land-use scenario (SUST-INEQ) is simulated to lead to a clear global cooling (Figures 4j, 4k, and 4l). This effect is apparent for all ESMs but is generally more pronounced in CESM and EC-EARTH, with local decreases up to 3°C in CESM and 1°C in EC-EARTH. This annual mean cooling is present in all seasons (see Appendix C). During northern hemisphere summer, the global cooling signal is least pronounced with even some regional warming of up to 1°C in CESM and EC-EARTH due to biogeophysical effects, such as albedo-induced warming over parts of the USA (Figure C4). The local biogeophysical cooling over the tropics is present throughout the year in all ESMs and is most pronounced during the northern hemisphere summer season.

3.2. Effects of Future Land-Use Scenarios on Heat Stress

The effects of the RCP1.9 scenario (futCTL-presCTL) on WBGT largely follow the same patterns as near-surface air temperature, with a global WBGT increase over land which is largest in CESM (1.2°C) and EC-EARTH (1°C) and lowest in MPI-ESM (0.37°C) (Figures 5a, 5b, 5c). In some regions, however, the changes to the other variables included in heat stress (near-surface wind, incoming surface shortwave radiation and relative/specific humidity) counteract the temperature effect. The annual mean maps for these variables are included in Appendix D. For CESM and MPI-ESM, the temperature cooling over the North Atlantic is causing the

nearby regions such as Northwestern Europe and Greenland to show no change in WBGT (Figures 5a and 5b). In the sustainable land-use scenario, areas with afforestation in higher latitudes, like Eastern USA, suffer from more heat stress, mirroring the patterns of warmer temperatures (Figures 5d, 5e, and 5f). The inequality scenario shows a global increase in heat stress (Figures 5g, 5h, and 5i), however the magnitude of this increase in WBGT is lower than for near-surface air temperature. This is especially clear over Central Africa, where the strong local warming in near-surface temperature (Figures 4g, 4h, and 4i) is not directly translated to increased heat stress in CESM and EC-EARTH and even shows a decrease of locally up to 0.5°C in MPI-ESM. Although irrigation has been shown to play an important role for moist heat stress (Mishra et al., 2020; Yao et al., 2024) the changes in irrigation extent in the LUC scenarios presented here (Figure B1) do not appear to translate into changes in heat stress. This could be explained by a prevalence of more humidity weighted metrics in studies on the impacts of irrigation on heat stress (a.o. wet bulb temperature), in contrast to the WBGT metric used here (Chakraborty et al., 2024).

Both CESM and EC-EARTH show a clear increase in heat stress in the RCP1.9 scenario which is in line with the geographic patterns of the temperature increase. In contrast, MPI-ESM shows less heat stress increases over low latitudes (Figures 5b and 5c). Interestingly, EC-EARTH shows a reduction in incoming surface shortwave radiation in Central Africa, while for CESM, there is a global increase in incoming surface shortwave radiation (Figure D4). MPI-ESM has the lowest value of Equilibrium Climate Sensitivity across the three ESMs and, consequently, shows the lowest influence of temperature on heat stress. Moreover, compared to the two other ESMs, MPI-ESM shows a WBGT cooling during northern hemisphere summer (JJA) in MPI-ESM of 0.5°C in some parts of Central Africa (Figure C5).

Both CESM and EC-EARTH show a moderate but widespread WBGT warming under the inequality scenario relative to the RCP1.9 scenario (Figure 5, for seasonal impacts see Figure C8). In both CESM and EC-EARTH, the increased heat stress over the tropics is consistent with an increase in both temperature and specific humidity (Figure D1) despite CESM becoming more windy (Figure D3). In contrast, MPI-ESM shows a heat stress reduction in some regions of Africa and Latin America (Figure 5h). This is consistent with the heat stress reducing effect due to an increase in wind speed and decreased specific humidity over those regions in MPI-ESM which counteract the increase in temperature and incoming surface shortwave radiation. For the sustainability scenario, all three ESMs show relatively small impacts on heat stress compared to the RCP1.9 scenario (Figures 5d, 5e, and 5f). Overall, the results show that achieving the sustainability scenario in favor of the inequality scenario (SUST-INEQ) leads to a general decrease in heat stress, except for the tropics in MPI-ESM where there is a slight increase in heat stress (Figures 5j, 5k, and 5l).

3.3. Impact on Labor Capacity

The increased heat stress for the RCP1.9 scenario (Figures 5a, 5b, and 5c) causes an increased impact on labor capacity over tropical regions (Figures 6a, 6b, and 6c). This spatial pattern is consistent with previous studies of higher warming scenarios (Orlov et al., 2020). Out of the three ESMs, CESM shows the largest and most widespread reduction in labor capacity. For instance, in some locations, the seasonal average labor capacity could decrease by up to 7%. In contrast to the other ESMs, MPI-ESM shows only small decreases with seasonally (JJA) even increases in average labor capacity of 2% over Central Africa (Figure C9).

Under the inequality scenario, both CESM and EC-EARTH show a reduction in labor capacity in low latitudes (Figures 6g and 6i). However, this reduction in labor capacity is small compared to changes under the RCP1.9 scenario, representing only 18% for CESM and 30% for EC-EARTH over the tropical latitudes (between 20°N and -20°S). In CESM, the reductions in the seasonal average labor capacity (Figure C11) are most pronounced in Latin America and Northern Australia (in DJF), and in the Sahel (in JJA). For EC-EARTH, Southeastern USA, China, and the Sahel experience relatively strong reductions in labor capacity during the northern hemisphere summer season (JJA). For MPI-ESM, in contrast, there is a clear increase in labor capacity as a consequence of the inequality scenario's deforestation in that region. In some locations in Africa, the seasonally averaged labor capacity could increase by even up to 4% points (Figure C11).

The sustainability scenario does not show any clear patterns for annual mean labor capacity (Figures 6d, 6e, and 6f) as the majority of the LUC in this scenario take place in the mid-latitudes (where labor capacity thresholds are less often exceeded). Remarkably, EC-EARTH shows a relatively strong and widespread reduction in labor capacity in Southeastern USA and China during the northern hemisphere summer season (JJA) of up to 2.5%

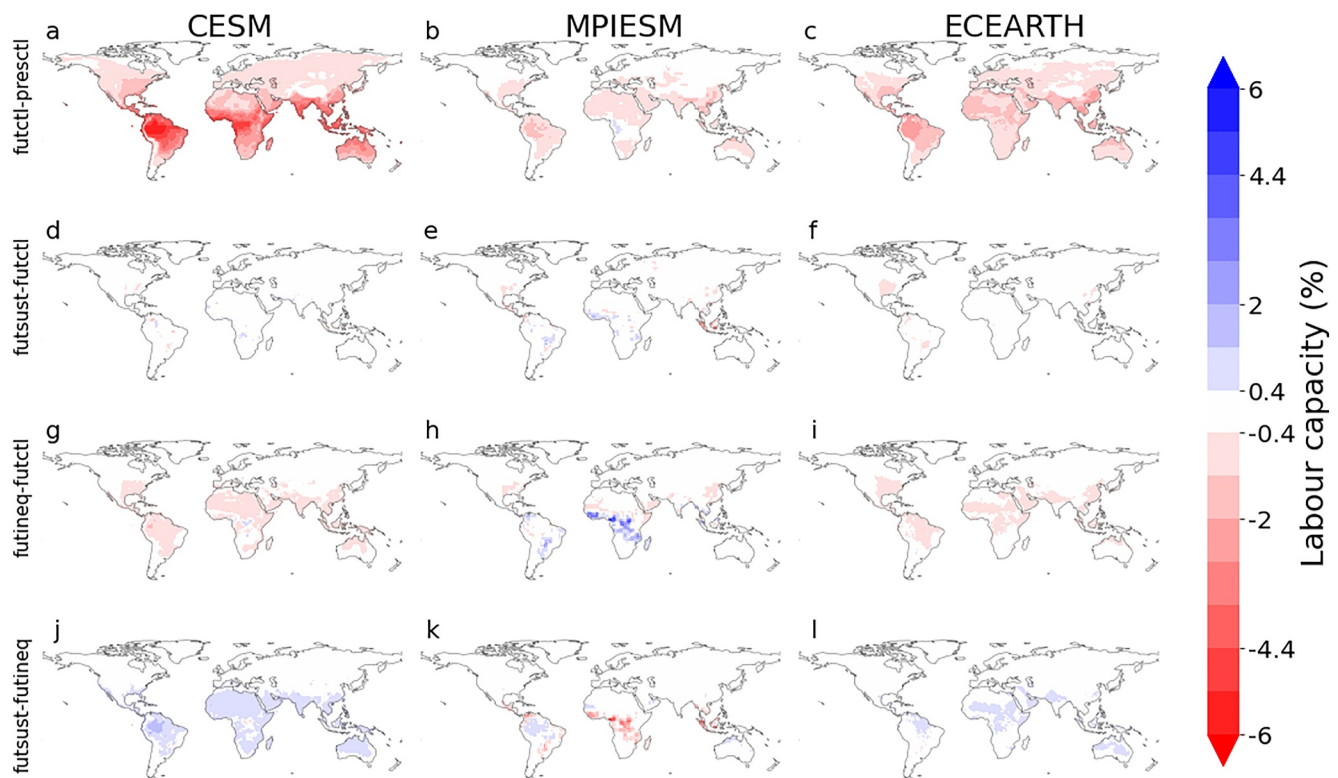


Figure 6. Changes in annual mean labor capacity (%) using the method presented in Havenith et al. (2024). Values were computed from WBGT over a 12hr work day (7a.m.- 7p.m.) by the end of the century (2070–2099) between the futCTL and presCTL scenarios, the sustainability and futCTL scenarios, the inequality and futCTL scenarios, and the sustainability and inequality scenarios, for CESM (a, d, g, j), MPI-ESM (b, e, h, k) and EC-EARTH (c, f, i, l), respectively.

(Figure C10), which is likely caused by an afforestation-induced increase in temperature (Figure C2) and a reduction in wind speed over that region (Figure D3).

Overall, the difference between the LUC scenarios (SUST-INEQ) causes contrasting responses over the tropics depending on the ESM, with a slight increase in labor capacity for EC-EARTH and CESM and a decrease for MPI-ESM (Figures 5g, 5h, and 5i). Hence, despite the consistent LUC-induced effects on temperature on a global scale (Figure 3) there are large differences in local impacts on labor capacity. This is further explained through the difference between warm extreme conditions (here illustrated by the 90th percentile) and mean conditions for near-surface air temperature and WBGT. These differences are illustrated here for Central Africa (Figure 7), as this region experiences large-scale LUC (Figure 2) and large responses in heat stress (Figure 5).

The effects on mean annual near-surface temperature (blue) and WBGT (orange) across all ESMs and land-use scenarios are similar with a slightly smaller magnitude on the effect for WBGT compared to near-surface temperature (Figures 7a, 7c, and 7e). There is the notable exception of MPI-ESM where the mean magnitude of the effect of near-surface temperature (which was negligible) increases when considering WBGT. However, when considering the warm extreme changes (90th percentile), it is clear that the effect of WBGT decreases in magnitude compared to the temperature response (i.e., there is a larger discrepancy between the temperature response and WBGT response). For the LUC scenarios, the difference in magnitude of extreme near-surface temperature and WBGT tends to be larger than the difference in magnitude of the monthly mean near-surface temperature and WBGT. This is likely related to the LUC-induced climate effects (local biogeophysical effects) being more pronounced during warm extreme conditions. The temperature effect is counteracted by an increase in wind speed (Figure D3). These effects appear to largely cancel each other out in CESM and EC-EARTH, causing the extreme WBGT effects to be close to zero. In MPI-ESM, in contrast, the specific humidity shows a decrease which counteracts the temperature effect, changing the sign and thus causing an increased labor capacity for deforestation under the inequality scenarios in that ESM (Figures 7c and 7d).

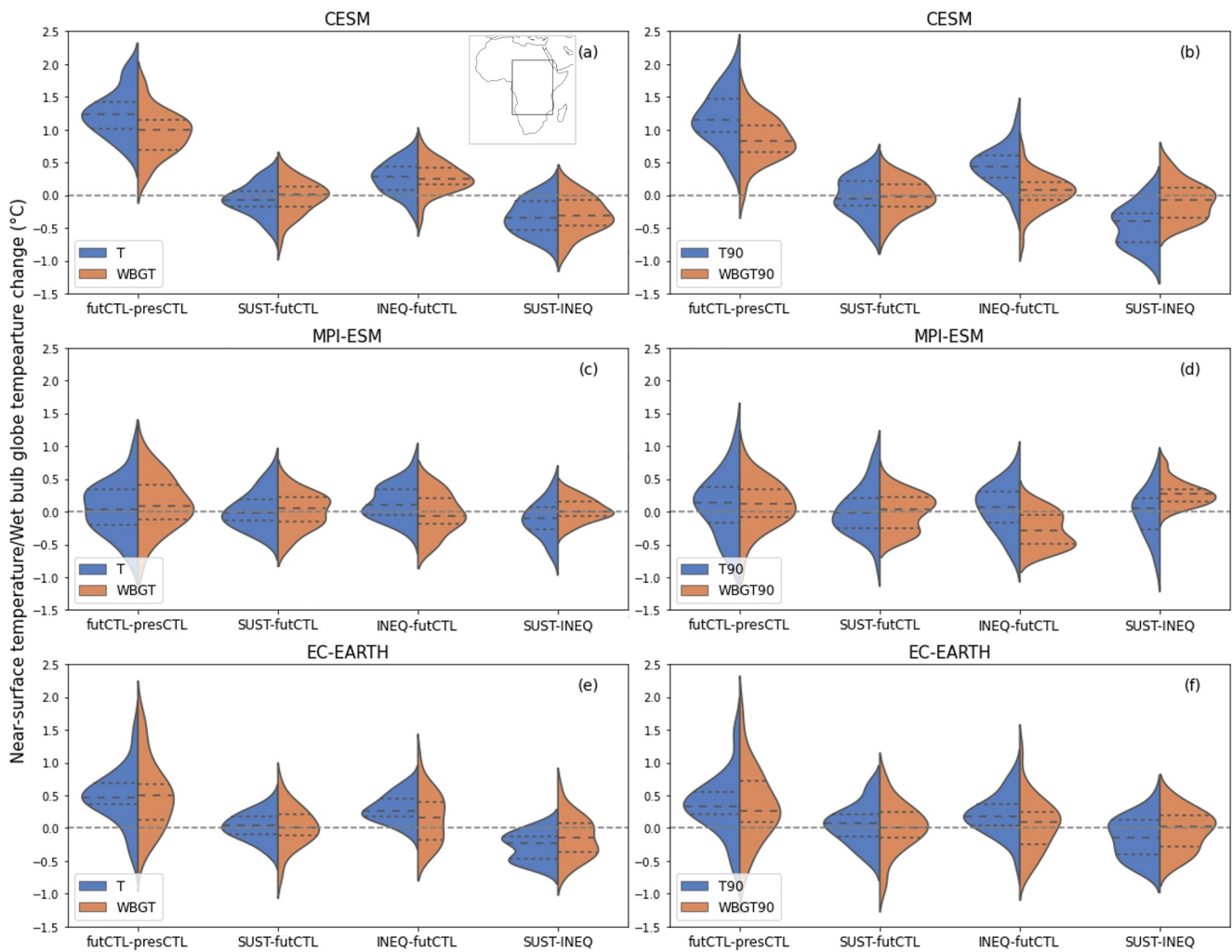


Figure 7. Probability Density Functions for annual average near-surface air temperature (T) and wet bulb globe temperature (WBGT) over Central Africa for all scenarios (futCTL-presCTL, SUST-futCTL, INEQ-futCTL, SUST-INEQ) for CESM (a), MPI-ESM (c) and EC-EARTH (e) and for the annual 90th percentile over Central Africa for CESM (b), MPI-ESM (d) and EC-EARTH (f). The violin plots show the median and the first and third quartile in stippled lines. Central Africa is defined between 20°N and 20°S and 10°E to 40°E as is shown in panel a.

4. Discussion

4.1. Implications for Mitigation and Adaptation Potential of Future LUC

The land use scenarios investigated in this study significantly impact GMT, revealing that future land use trajectories may determine whether the global warming levels of 1.5°C and 2°C will be exceeded or not, if fossil fuel emissions remain limited to levels compatible with these targets. Within the simulations presented here, the ensemble mean response of two ESMs exceed the 1.5°C threshold averaged over the period 2069–2099 and in the inequality scenario even the 2°C warming threshold is surpassed in those ESMs. The sustainability LUC scenario is simulated to a lower future warming compared to the inequality LUC scenario in each ESM (Figure 4), highlighting the importance of well-informed land-based mitigation decisions for reaching global temperature targets.

In contrast to the GMT mitigation potential of the different LUC scenarios, our ESM simulations highlight more uncertainty in the potential to mitigate local heat stress and downstream effects on labor capacity in the tropical regions. There exist clear differences between the LUC-induced effects on heat stress and those for temperature, especially over regions of large-scale LUC such as Central Africa. This can be explained by the canceling out of different biogeophysical effects (e.g., temperature vs. specific humidity) during extremes when the exposure to

Table 1

Overview of the Biogeophysical Effects Across the ESMs for the Two Main LUC Patterns: Tropical Deforestation and Northern Hemisphere (NH) Afforestation

Scenario	Inequality	Sustainability
Land-Use Change	Tropical deforestation	NH afforestation
T	Clear increase	Rather increase
Q	Inconsistent	Inconsistent
RH	Clear decrease	Inconsistent
U	Clear increase	Clear decrease
S_{down}	Inconsistent	Inconsistent
WBGT	Rather increase	Clear increase

Note. The variables considered are those relevant for heat stress as computed by the Wet Bulb Globe Temperature (WBGT): near-surface temperature (T), Specific Humidity (Q), Relative Humidity (RH), Wind speed (U) and incoming surface shortwave radiation (S_{down}).

heat stress is especially strong (Figure 7). This clearly highlights that the adaptation potential of LUC might be more limited than previously suggested due to biogeophysical effects (Chausson et al., 2020; Jia et al., 2019).

These implications are only valid for the end of the century period. However, as the LUC scenarios include LUC throughout the century, the differences in LUC and thus their climate effects were simulated to be even smaller around the mid-century period (see Appendix E). While at the same time global warming will peak over the mid-century within RCP1.9 scenarios (see Table E1) (Rogelj et al., 2018). The delayed response of the LUC-induced climate effects further highlights the limited adaptation potential of LUC for Paris Agreement compatible scenarios as the LUC-induced climate effects would possibly only become substantial after the warming peak has already passed.

In general, our results highlight greater importance of avoiding tropical deforestation compared to NH afforestation. In fact, compared to futCTL, the sustainability scenario does not show substantial climate benefits related to temperature or heat stress in most ESMs used in this study. This is in line with a previous study analyzing these simulations for temperature-related mortality (Orlov, De Hertog et al., 2024). However, beyond climate-induced effects, the assumptions embedded within the scenario clearly indicate that pursuing the path of the sustainability scenario provides several important co-benefits for the socio-economic development of low- and middle-income countries as well as to nutrition, ecosystem conservation, nitrogen pollution and agricultural water use (Humpenöder et al., 2022).

4.2. Local Biogeophysical Interactions Influence Heat Stress

Our results clearly show the importance of including variables beyond temperature for assessing LUC impacts on heat stress, as the LUC-induced biogeophysical effects on specific humidity and wind speed substantially determine the effect on WBGT. These biogeophysical effects are dependent on the type of LUC and the region where they are applied, with important discrepancies between the mid-latitudes and the tropics (De Hertog et al., 2023; Duveiller et al., 2018). The future LUC scenarios presented here, show two main LUC patterns: northern hemisphere afforestation (mostly sustainability scenario) and tropical deforestation (inequality scenario). With regard to heat stress, the temperature increase due to tropical deforestation (Figure 4) is counteracted by an increase in wind speed which is consistent across all ESMs and by a decrease in humidity in MPI-ESM. Regarding northern hemisphere afforestation, the effects on both specific humidity and wind speed are less consistent across the ESMs and thus also less consistent for the effects on heat stress. The different variables incorporated in the WBGT calculation and their sign of change are summarized in Table 1. These changes in the biogeophysical variables can give an indication of their potential role in the resulting heat stress. However, to fully quantify the importance of the changes in these different variables a systematic analysis should be performed, for instance following the framework proposed by Kong and Huber (2024a). However, this is beyond the scope of the present study.

The representation of LUC-induced biogeophysical effects remains uncertain across ESMs (Boysen et al., 2020; De Hertog et al., 2024). For example, CESM overestimates the albedo change following deforestation in boreal latitudes (De Hertog et al., 2023). Another feature of this ESM is a strong sensitivity of the Atlantic Meridional Overturning Circulation (AMOC) to temperature changes (e.g., Portmann et al., 2022). Furthermore, CESM and EC-EARTH do not capture the diurnal cycle of LUC-induced effects well compared to observational data (Duveiller et al., 2018), which could lead to a misinterpretation of the severity of heat stress and the downstream labor capacity effects as these are computed over the local daytime (Orlov, De Hertog et al., 2023).

In this study we assessed heat stress through the WBGT using the Liljegren method (Liljegren et al., 2008). However, we also calculated a commonly used proxy, which is the computationally less expensive ESI. This metric has been shown to be a valid approximation for annual or seasonal mean heat stress (Kong & Huber, 2022). For the futCTL scenario (RCP1.9), the ESI heat index is comparable in the magnitude with WBGT and consistent in terms of sign across ESMs. However, when using ESI, the effects on heat stress and associated impacts on labor capacity strongly differ over the areas of large-scale LUC, such as Central Africa (Figure F1 and F2). When considering ESI instead of WBGT, the inequality scenario does not show any increase in labor capacity for MPI-

ESM (Figure F2). These results indicate that the notion that ESI is a good alternative to WBGT does not hold for LUC-induced climate effects. This is likely due to the complex interactions between the various biogeophysical effects (such as on wind speed and specific humidity) caused by the LUC. Our findings underline the need to use more sophisticated heat stress indices, such as WBGT, when analyzing the heat stress impacts of LUC-based scenarios.

4.3. Limitations and Future Research

Our analysis is subject to several limitations, which can be addressed in future research. Firstly, we focus only on the impact on heat stress and labor capacity, while a LUC-induced local climate change could also affect health, crop productivity, biodiversity, and livestock productivity among others (Orlov, Aunan, et al., 2023). Future research should take a broader perspective to assess the total cost and the distributional impacts of different LUC scenarios on the society. The method for computing labor capacity by Havenith et al. (2024) provides a data based estimate of the relationship between heat stress and impacts on labor. This likely represents a more accurate representation of labor capacity impacts than the safety standards based on NIOSH as is often used in ESM-based studies on the topic (a.o. De Lima et al., 2021; Orlov, De Hertog et al., 2023). The NIOSH recommendations tend to be more cautious for high WBGT values, therefore leading to generally higher impacts on labor capacity (see Figure G1). However, despite using an empirically based relationship between WBGT and labor capacity this quantification remains merely an indication of actual impacts, as local temperatures at the site of work can vary considerably from grid scale averages of 100×100 km as produced by ESMs. Finally, only impacts on labor capacity due to humid heat are considered here while effects due to increased/decreased cold are neglected (Orlov, De Hertog et al., 2023).

Moreover, LUC does not only affect the climatic conditions through biogeochemical and biogeophysical effects (i.e., hazard) but can also affect the exposure and vulnerability to heat stress. Specifically, in our scenario setting, a more sustainable LUC assumes more afforestation by the cost of less areas for crop production (Figure 2), which also implies that less people will be working in crop production and consequently be exposed to heat stress. Furthermore, our global sustainability narrative assumes inclusive socio-economic development and a rapid technological diffusion in low- and middle-income countries, which also imply agricultural intensification and a reduction in the vulnerability to heat stress impacts (e.g., mechanization deployment) (Orlov et al., 2020, 2021).

ESMs as a modeling tool that are run at a low spatial resolution are limited in their representation of fine scale processes which could be highly relevant for assessing heat stress. For example, the effects of LUC on nearby urban areas is not explicitly represented at this scale, despite urban areas being hotspots for heat stress (Oleson et al., 2015; Wouters et al., 2017). The use of more fine-scale modeling tools such as regional climate models for this type of research could help narrow down the remaining uncertainties, although they would have to be applied over multiple domains. Additionally, we only performed the dedicated simulations with three ESMs while previous research suggests that inter-ESM variability related to LUC-induced climate effects is substantial, both relating to biogeophysical and biogeochemical effects (Boysen et al., 2020).

The scenarios and simulations presented here provide yet another illustration of the importance of considering LUC when studying the future climate. In particular, this is to our knowledge the first study demonstrating that the future global land-use trajectory that societies will embark on could play a crucial role in determining whether the long-term temperature goal of the Paris Agreement will be exceeded or not, even if fossil fuel emissions are kept at levels previously assessed to be compatible with this outcome. However, our analysis is limited to temperature-induced climate effects and does not cover a full description and interpretation of all processes driving the biogeochemical and biogeophysical LUC-induced temperature effects presented here. These scenarios could also be analyzed for their development over time in order to assess potential characteristics such as temperature overshoot and how these might be affected by different LUC-scenarios. In addition, other climate-relevant variables such as terrestrial carbon and water storage and their respective land-atmosphere exchange and atmospheric teleconnections could be considered to further constrain potential impacts categories such as droughts and heat waves. Finally, these simulations can act as training and validation material for computationally light emulators such as MESMER (Beusch et al., 2020; Nath et al., 2022) and the recently developed component for the local biogeophysical effects of LUC (Nath et al., 2023, TIMBER) which allows for a more flexible assessment of different LUC scenarios under different climate scenarios.

5. Conclusion

Here we present Earth System Model (ESM) simulations dedicated to disentangling the effects of Land Use Change (LUC) under the low-warming RCP1.9 scenario. We use two contrasting LUC scenarios developed by Humpenöder et al. (2022) with vastly different socioeconomic assumptions: a sustainable future, where forests are preserved and planted, and a global inequality scenario, where large-scale tropical deforestation occurs due to cropland expansion. The climate projections are generated with the Community Earth System Model (CESM), the Max-Planck Institute Earth System Model (MPI-ESM) and the European Consortium Earth System Model (EC-EARTH). The ESMs are run in fully coupled, emission-driven mode, and the experiments were designed such that they can disentangle the LUC-induced climatic effects toward the end of the century as well as their impacts on human heat stress and labor capacity.

We show that avoiding the inequality land-use scenario and achieving the sustainability land-use scenario substantially alters global climate with a global mean temperature decrease of 0.10°C–0.35°C by the end of the century. Due to these global changes in temperature, an almost global reduction in heat stress over land is visible by the end of the century. However, the LUC impacts on labor capacity do not consistently mirror the changes in heat stress. Specifically over the tropical regions local biogeophysical effects on specific humidity and wind speed affect the LUC-induced effects on heat stress and even cause a decreased labor capacity according to one ESM. During warm extremes, the LUC-induced cooling gets counteracted by the biogeophysical feedbacks on wind speed and humidity which cause the effect on heat stress and consequent impacts such as labor capacity to be small.

These results are a clear illustration of the importance of LUC-induced climate responses for achieving the Paris Agreement goals of limiting global temperature to “well below 2°C and pursuing efforts to limit it to 1.5°C” (UNFCCC, 2015). However, when considering LUC for adapting to climate change effects locally, their potential is more uncertain and more limited due to local biogeophysical effects limiting the heat stress reduction, especially during extreme conditions when it matters most.

Appendix A: Land Use Implementations in ESMs

Figure A1

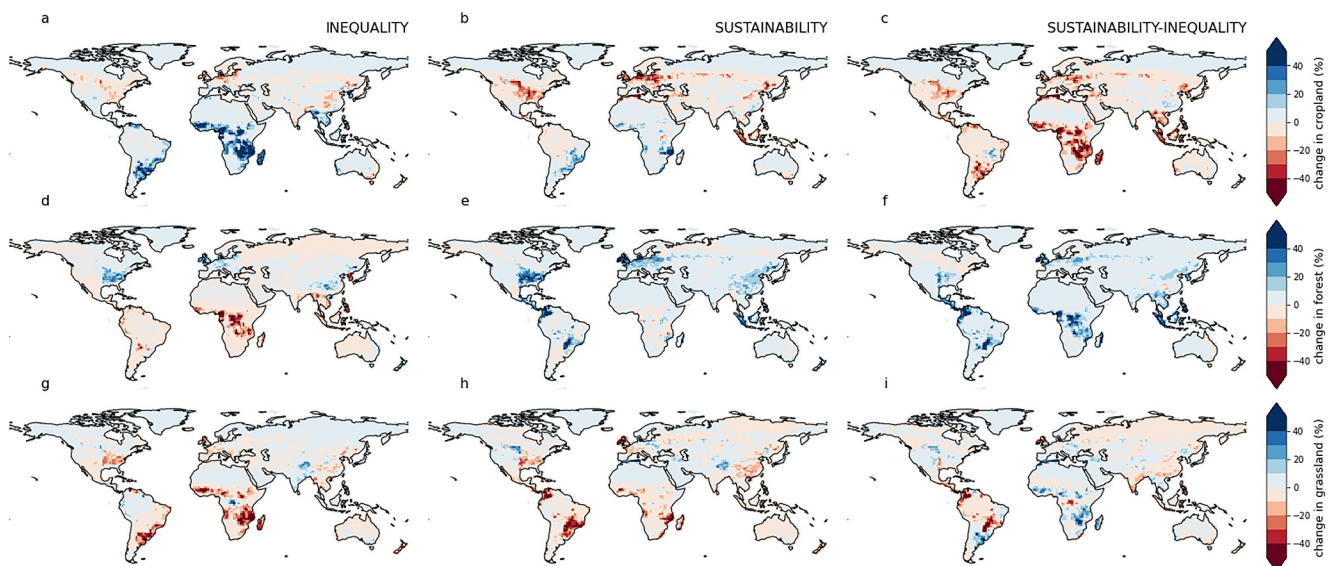


Figure A1. Land-use changes implemented in CESM showing the amount of cropland (a–c), forest (d–f) and grassland (g–i) changes as a grid cell fraction (%) within the inequality scenario (a, d, g), sustainability scenario (b, e, h) at the end of the century compared to the 2014 land use, and between the sustainability and inequality scenarios at the end of the century (c, f, i).

Figure A2

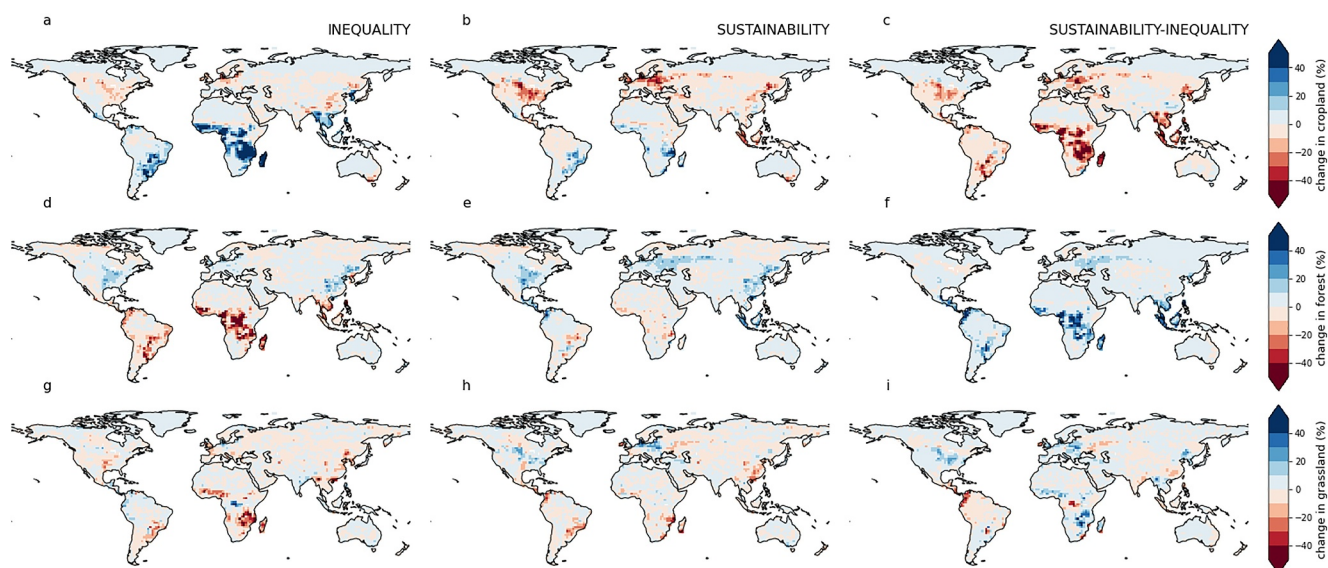


Figure A2. Land-use changes implemented in MPI-ESM showing the amount of cropland (a–c), forest (d–f) and grassland (g–i) changes as a grid cell fraction (%) within the inequality scenario (a, d, g), sustainability scenario (b, e, h) at the end of the century compared to the 2014 land use, and between the sustainability and inequality scenarios at the end of the century (c, f, i).

Appendix B: Changes in Irrigation Extent in CESM

Figure B1

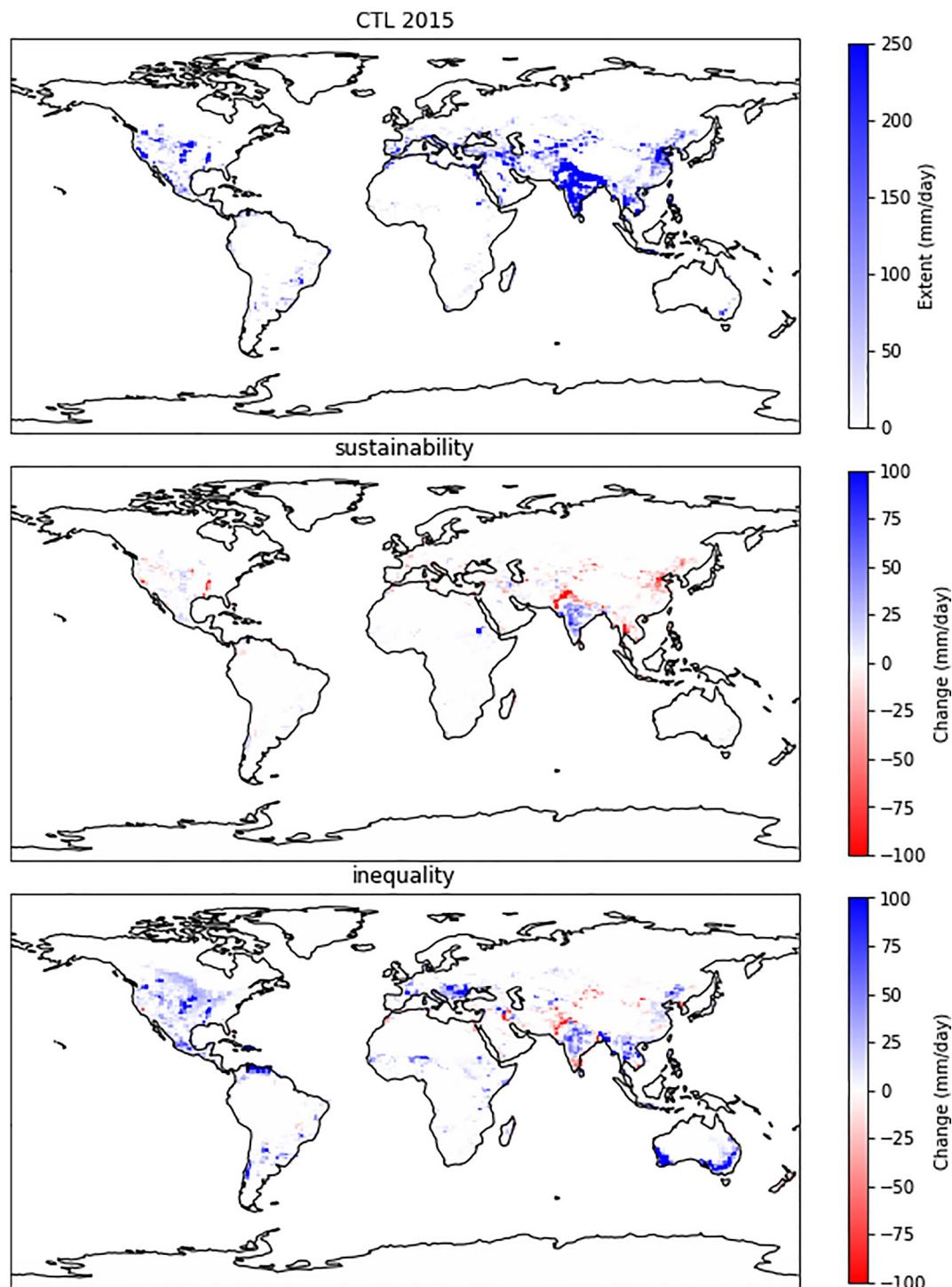


Figure B1. Irrigation extent during the CTL simulation in CESM (year 2015) and the changes in extent by the end of the century (2100) under the sustainability and inequality scenarios.

Appendix C: Seasonal Maps of Near-Surface Temperature, Wet Bulb Globe Temperature and Labor Capacity

Figure C1

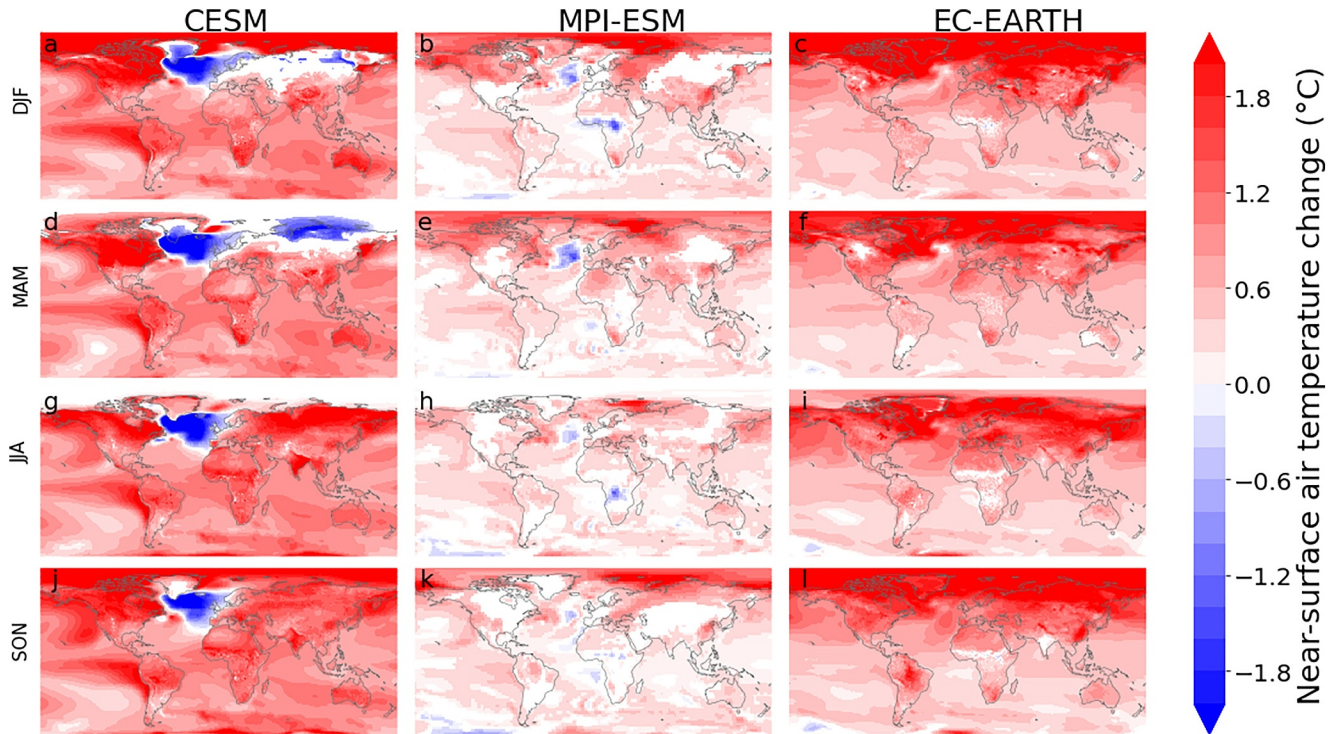


Figure C1. Seasonal averaged near-surface air temperature for the three ESMs for the RCP1.9 scenario (futCTL-presCTL). For CESM, MPI-ESM and EC-EARTH respectively the northern hemisphere spring (MAM) seasonal average (a, b, c), summer (JJA) seasonal average (d, e, f), fall (SON) seasonal average (g, h, i) and the winter (DJF) seasonal average (j, k, l). Only statistically significant changes are shown (0.05 significance level, two-sided Wilcoxon signed rank test of lumped ensemble members and field significance using the false discovery rate test).

Figure C2

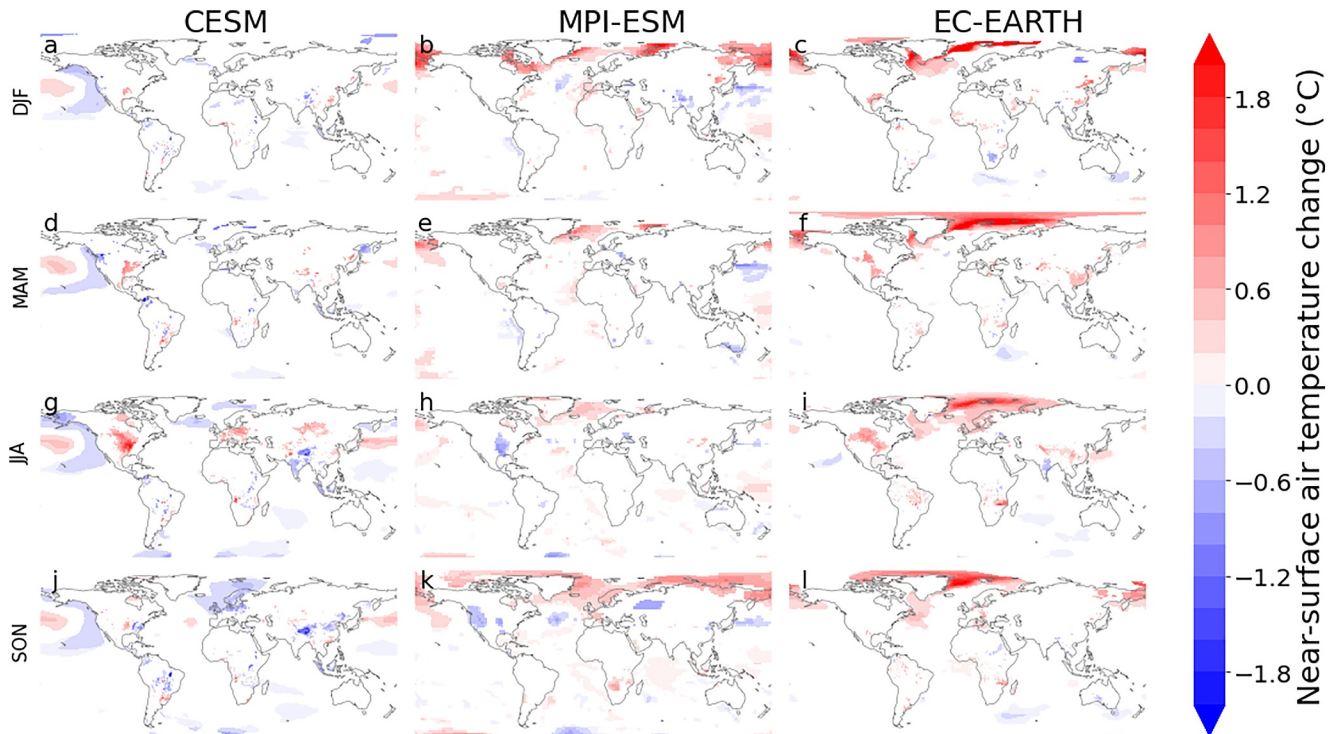


Figure C2. Seasonal averaged near-surface air temperature for the three ESMs for the sustainability scenario (SUST-futCTL). For CESM, MPI-ESM and EC-EARTH respectively the northern hemisphere spring (MAM) seasonal average (a, b, c), summer (JJA) seasonal average (d, e, f), fall (SON) seasonal average (g, h, i) and the winter (DJF) seasonal average (j, k, l). Only statistically significant changes are shown (0.05 significance level, two-sided Wilcoxon signed rank test of lumped ensemble members and field significance using the false discovery rate test).

Figure C3

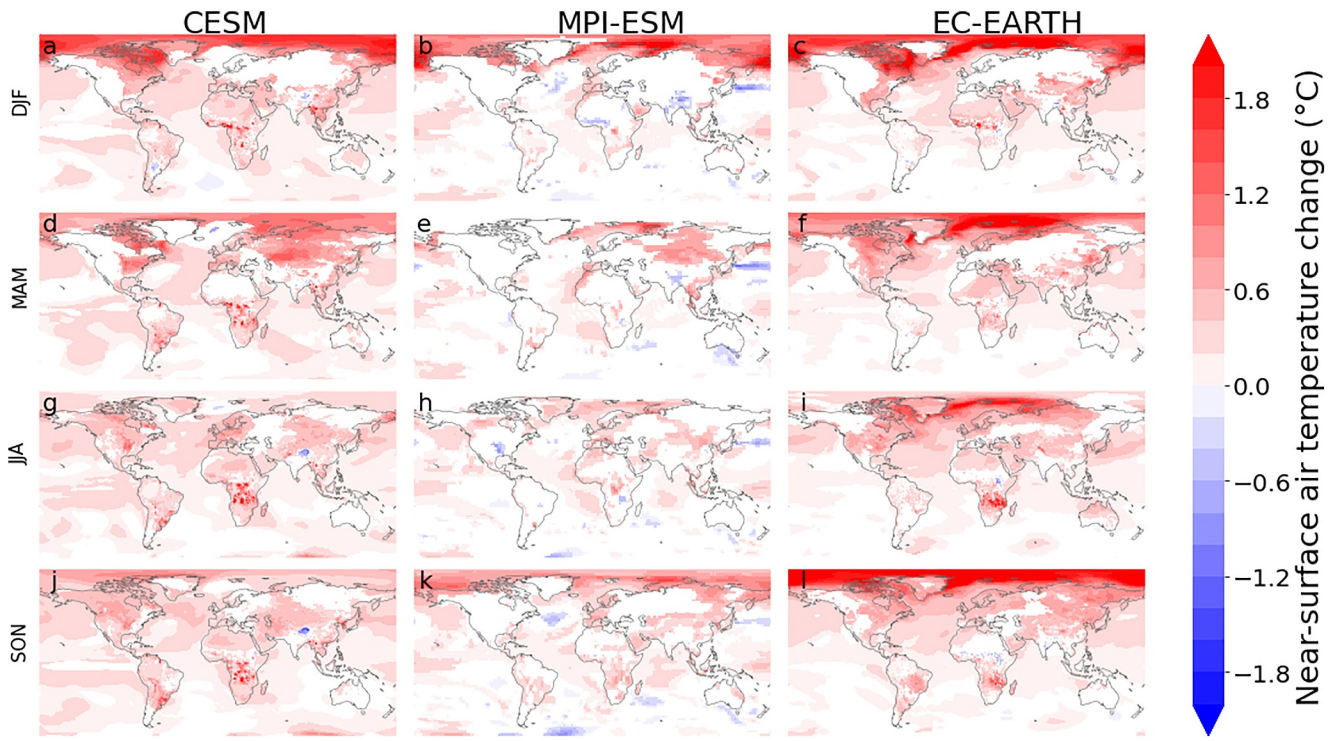


Figure C3. Seasonal averaged near-surface air temperature for the three ESMs for the inequality scenario (INEQ-futCTL). For CESM, MPI-ESM and EC-EARTH respectively the northern hemisphere spring (MAM) seasonal average (a, b, c), summer (JJA) seasonal average (d, e, f), fall (SON) seasonal average (g, h, i) and the winter (DJF) seasonal average (j, k, l). Only statistically significant changes are shown (0.05 significance level, two-sided Wilcoxon signed rank test of lumped ensemble members and field significance using the false discovery rate test).

Figure C4

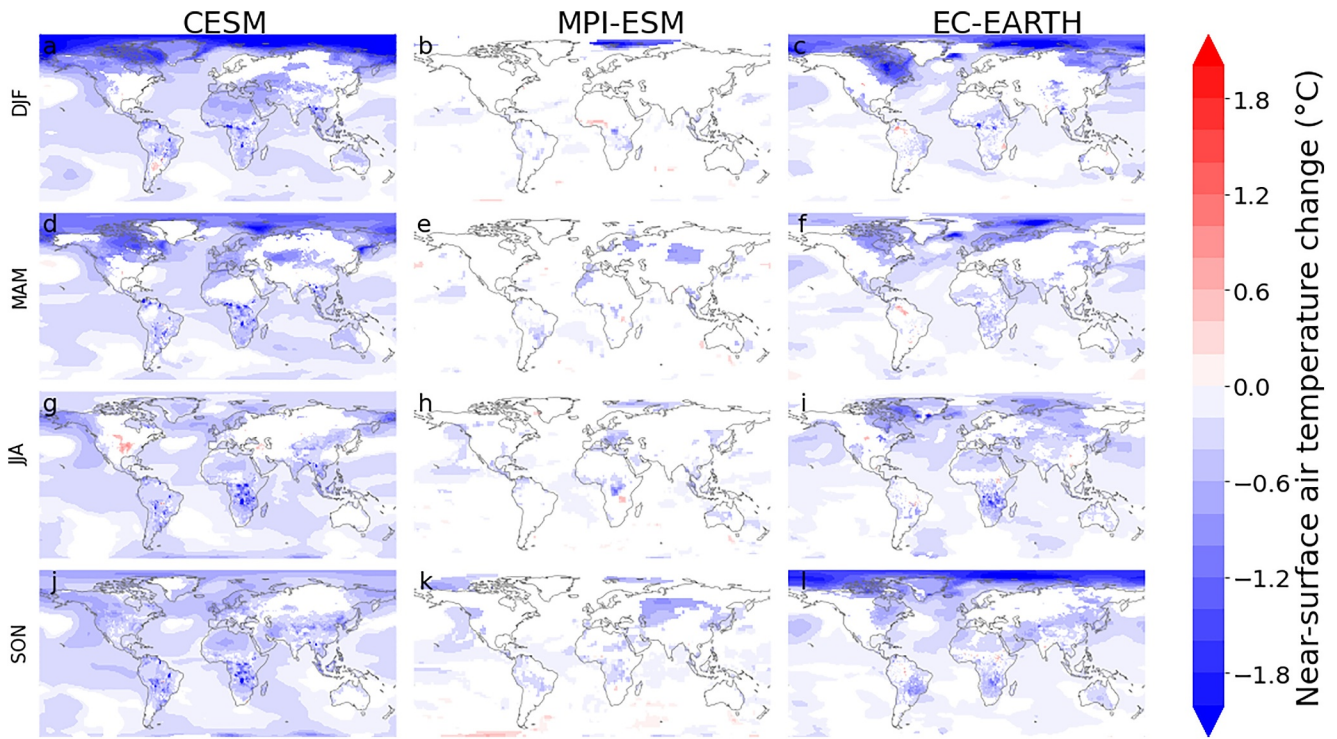


Figure C4. Seasonal averaged near-surface air temperature for the three ESMs for the SUST-INEQ case. For CESM, MPI-ESM and EC-EARTH respectively the northern hemisphere spring (MAM) seasonal average (a, b, c), summer (JJA) seasonal average (d, e, f), fall (SON) seasonal average (g, h, i) and the winter (DJF) seasonal average (j, k, l). Only statistically significant changes are shown (0.05 significance level, two-sided Wilcoxon signed rank test of lumped ensemble members and field significance using the false discovery rate test).

Figure C5

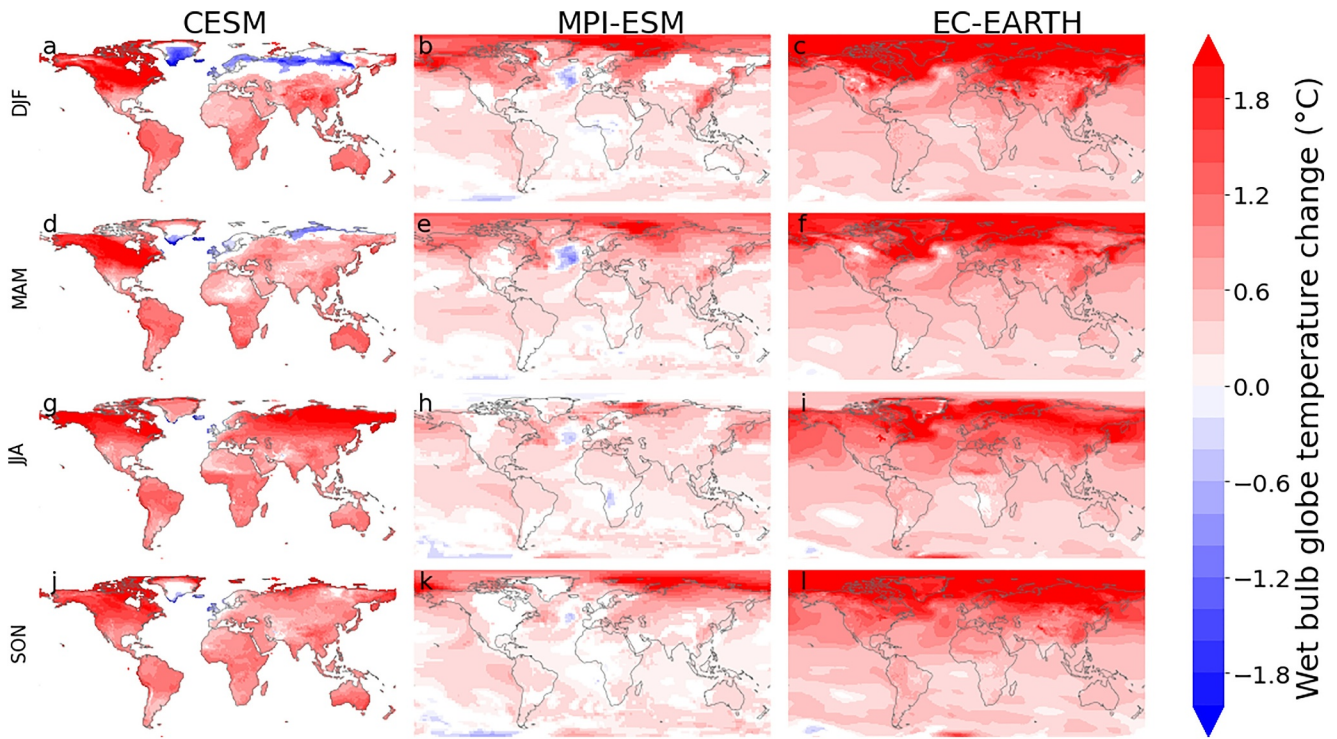


Figure C5. Seasonal averaged wet bulb globe temperature for the three ESMs for the RCP1.9 scenario (futCTL-presCTL). For CESM, MPI-ESM and EC-EARTH respectively the northern hemisphere spring (MAM) seasonal average (a, b, c), summer (JJA) seasonal average (d, e, f), fall (SON) seasonal average (g, h, i) and the winter (DJF) seasonal average (j, k, l). Only statistically significant changes are shown (0.05 significance level, two-sided Wilcoxon signed rank test of lumped ensemble members and field significance using the false discovery rate test).

Figure C6

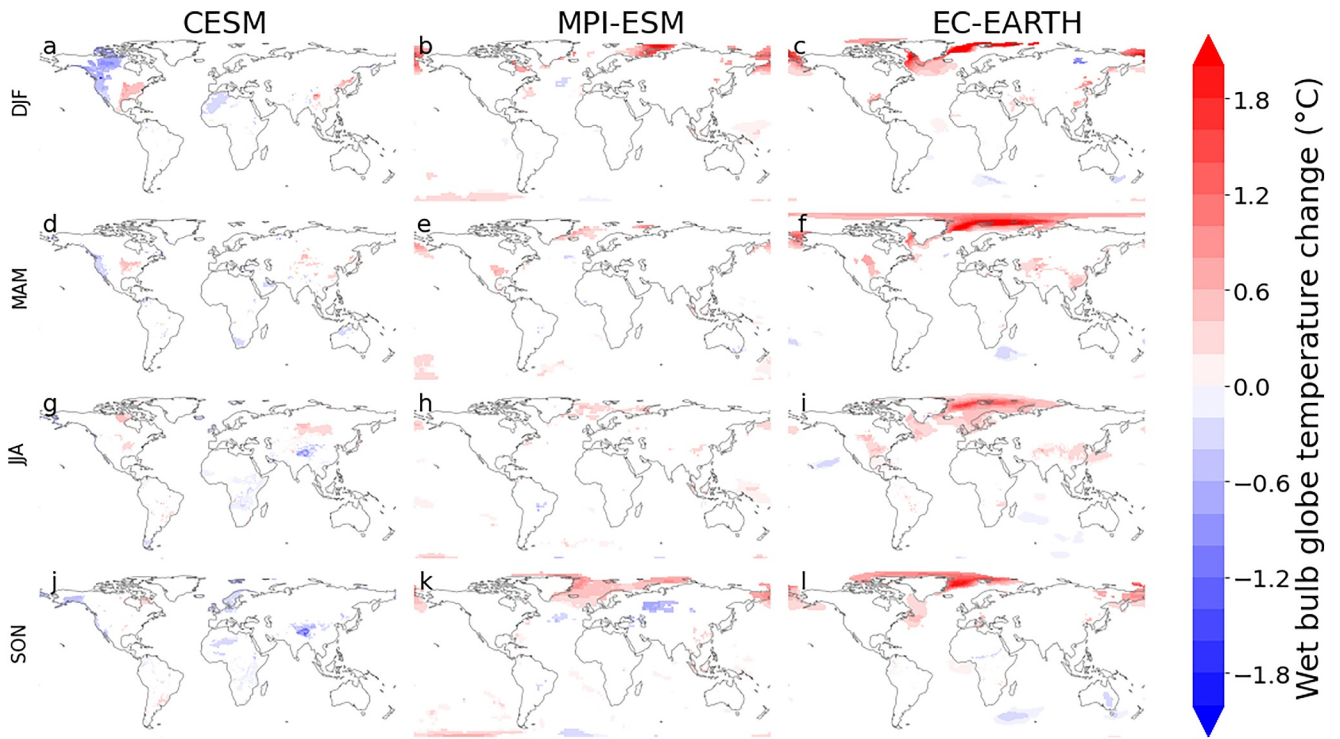


Figure C6. Seasonal averaged wet bulb globe temperature for the three ESMs for the inequality scenario (INEQ-futCTL). For CESM, MPI-ESM and EC-EARTH respectively the northern hemisphere spring (MAM) seasonal average (a, b, c), summer (JJA) seasonal average (d, e, f), fall (SON) seasonal average (g, h, i) and the winter (DJF) seasonal average (j, k, l). Only statistically significant changes are shown (0.05 significance level, two-sided Wilcoxon signed rank test of lumped ensemble members and field significance using the false discovery rate test).

Figure C7

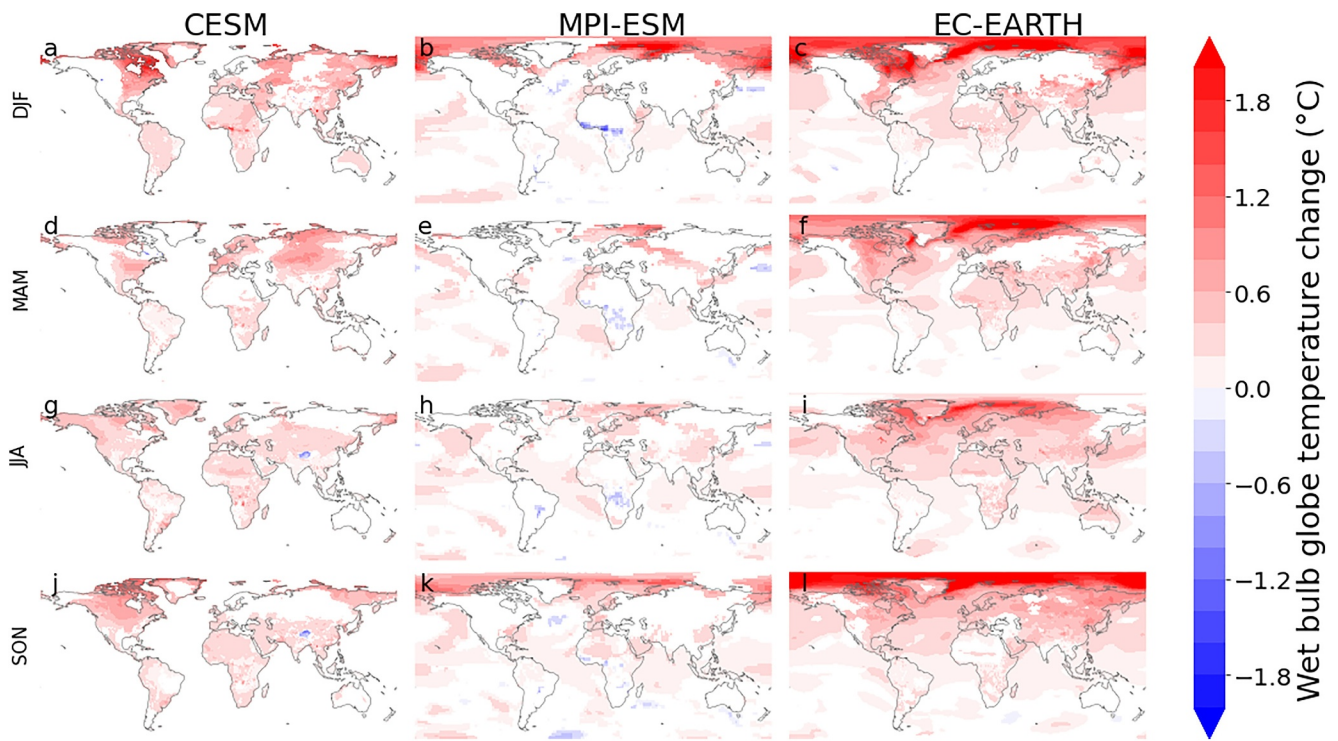


Figure C7. Seasonal averaged wet bulb globe temperature for the three ESMs for the sustainability scenario (SUST-futCTL). For CESM, MPI-ESM and EC-EARTH respectively the northern hemisphere spring (MAM) seasonal average (a, b, c), summer (JJA) seasonal average (d, e, f), fall (SON) seasonal average (g, h, i) and the winter (DJF) seasonal average (j, k, l). Only statistically significant changes are shown (0.05 significance level, two-sided Wilcoxon signed rank test of lumped ensemble members and field significance using the false discovery rate test).

Figure C8

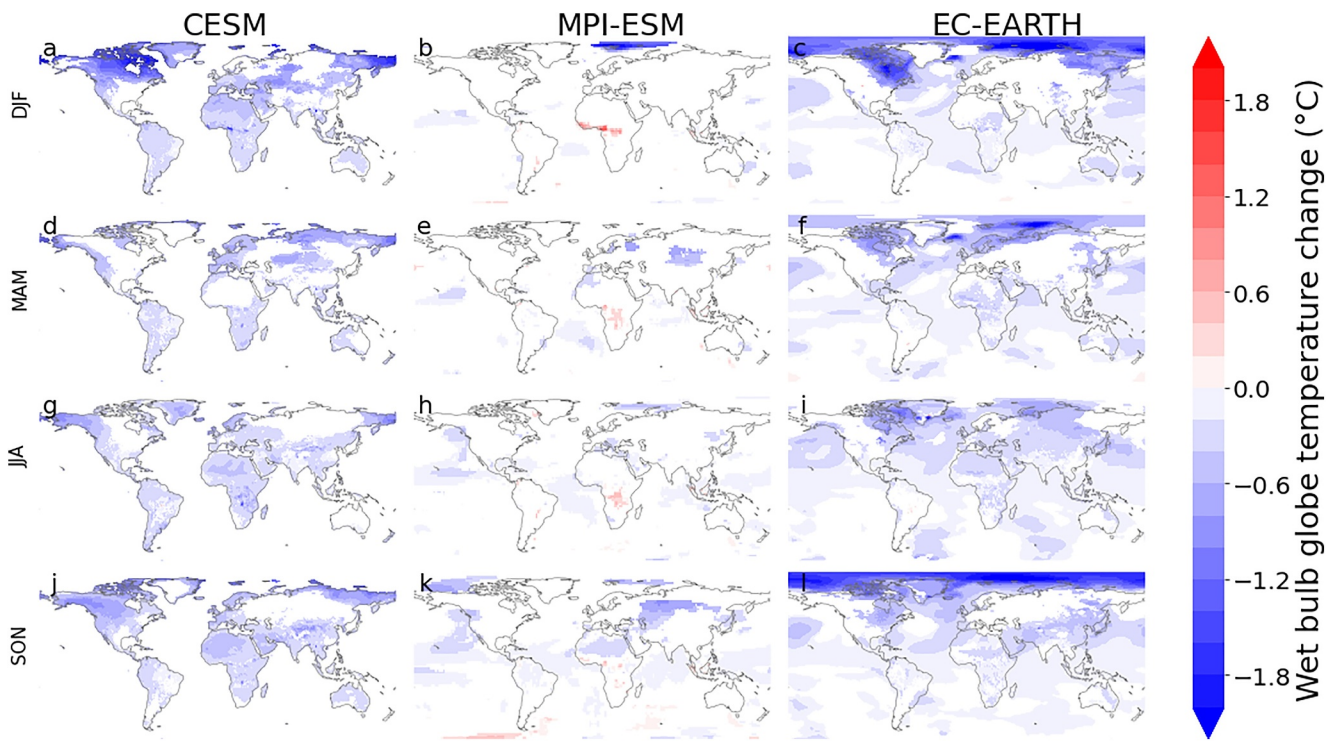


Figure C8. Seasonal averaged wet bulb globe temperature for the three ESMs for the SUST-INEQ case. For CESM, MPI-ESM and EC-EARTH respectively the northern hemisphere spring (MAM) seasonal average (a, b, c), summer (JJA) seasonal average (d, e, f), fall (SON) seasonal average (g, h, i) and the winter (DJF) seasonal average (j, k, l). Only statistically significant changes are shown (0.05 significance level, two-sided Wilcoxon signed rank test of lumped ensemble members and field significance using the false discovery rate test).

Figure C9

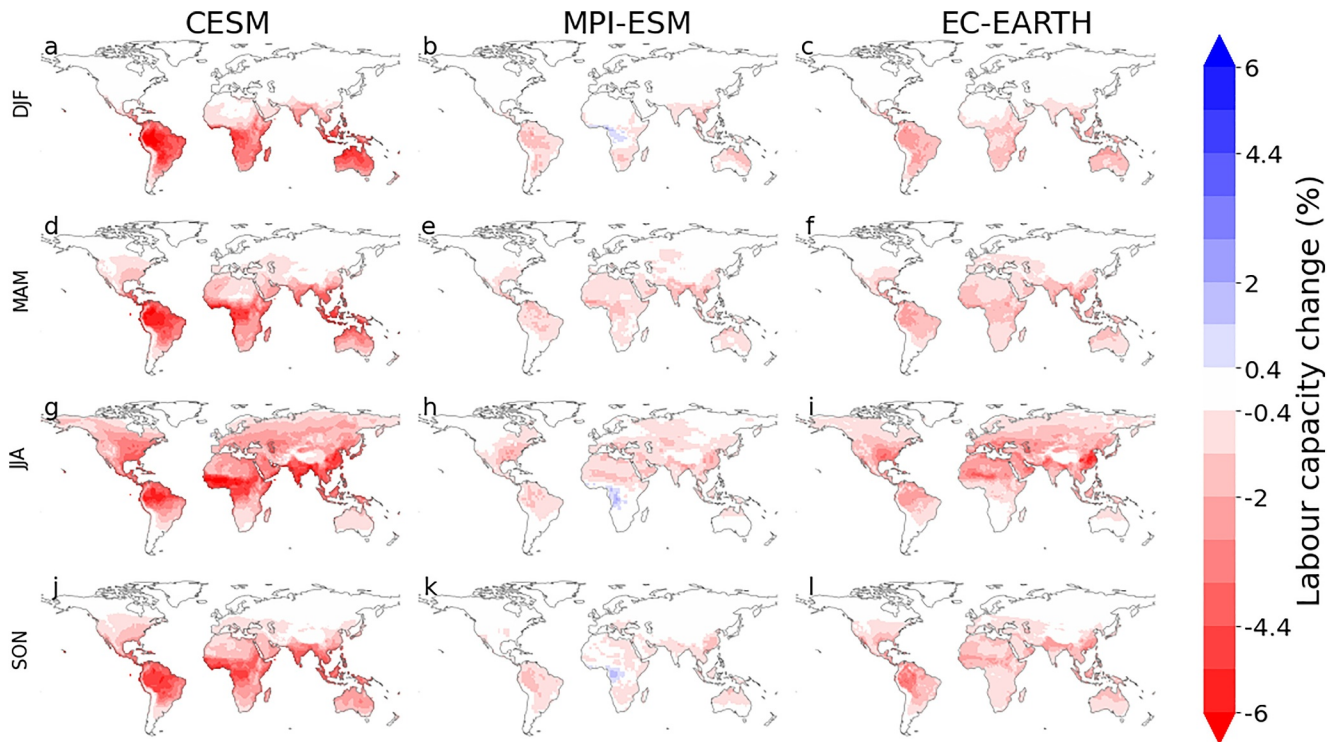


Figure C9. Seasonal averaged labor capacity (%) using the method presented in Havenith et al. (2024) for the three ESMs for the RCP1.9 scenario (futCTL-presCTL). For CESM, MPI-ESM and EC-EARTH respectively the northern hemisphere spring (MAM) seasonal average (a, e, i), summer (JJA) seasonal average (b, f, j), fall (SON) seasonal average (c, g, k) and the winter (DJF) seasonal average (d, h, l).

Figure C10

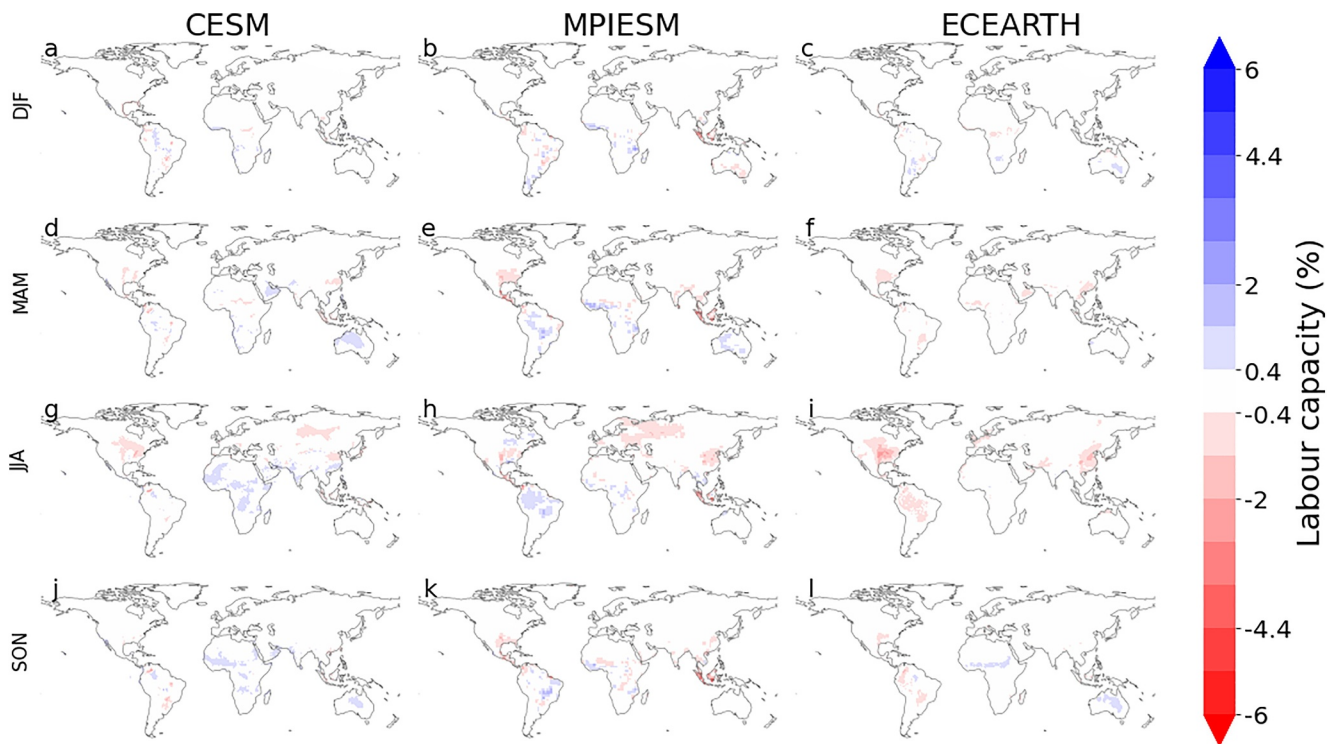


Figure C10. Seasonal averaged labor capacity (%) using the method presented in Havenith et al. (2024) for the three ESMS for the sustainability scenario (SUST-futCTL). For CESM, MPI-ESM and EC-EARTH respectively the northern hemisphere spring (MAM) seasonal average (a, e, i), summer (JJA) seasonal average (b, f, j), fall (SON) seasonal average (c, g, k) and the winter (DJF) seasonal average (d, h, l).

Figure C11

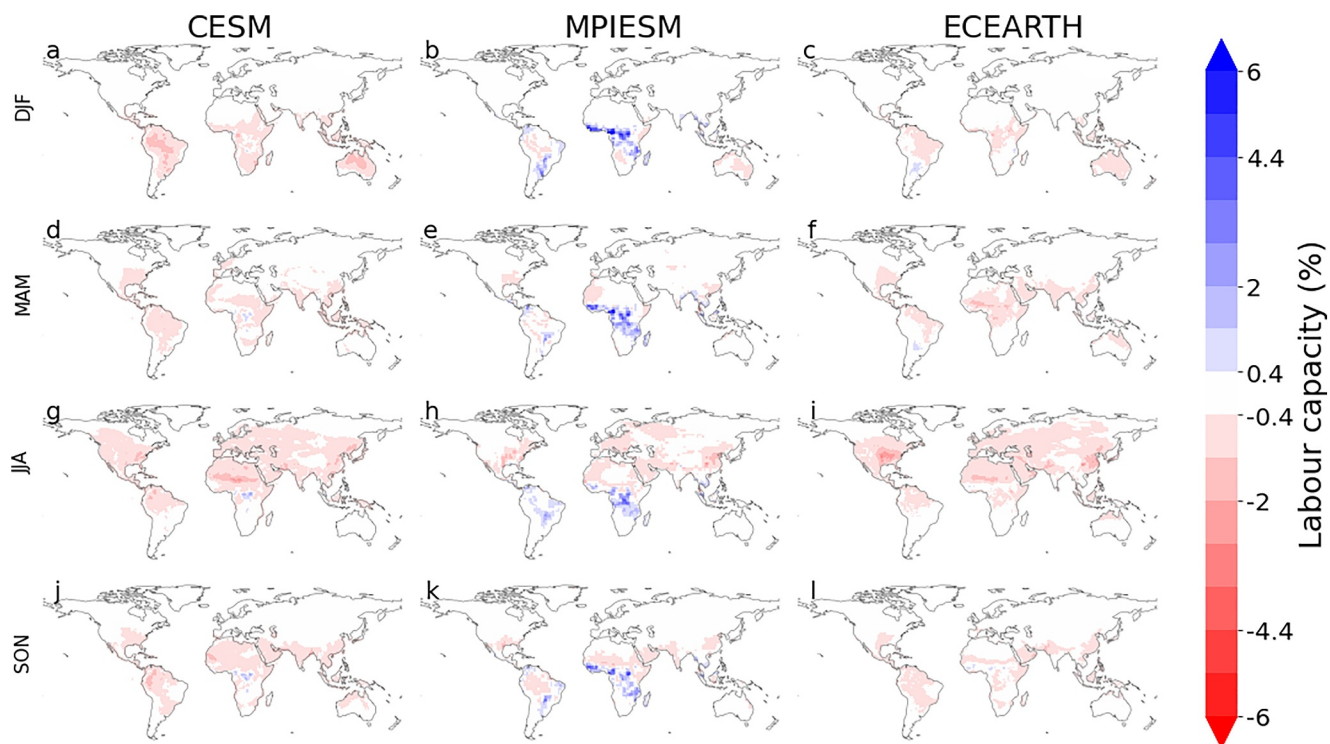


Figure C11. Seasonal averaged labor capacity (%) using the method presented in Havenith et al. (2024) for the three ESMs for the inequality scenario (INEQ-futCTL). For CESM, MPI-ESM and EC-EARTH respectively the northern hemisphere spring (MAM) seasonal average (a, e, i), summer (JJA) seasonal average (b, f, j), fall (SON) seasonal average (c, g, k) and the winter (DJF) seasonal average (d, h, l).

Figure C12

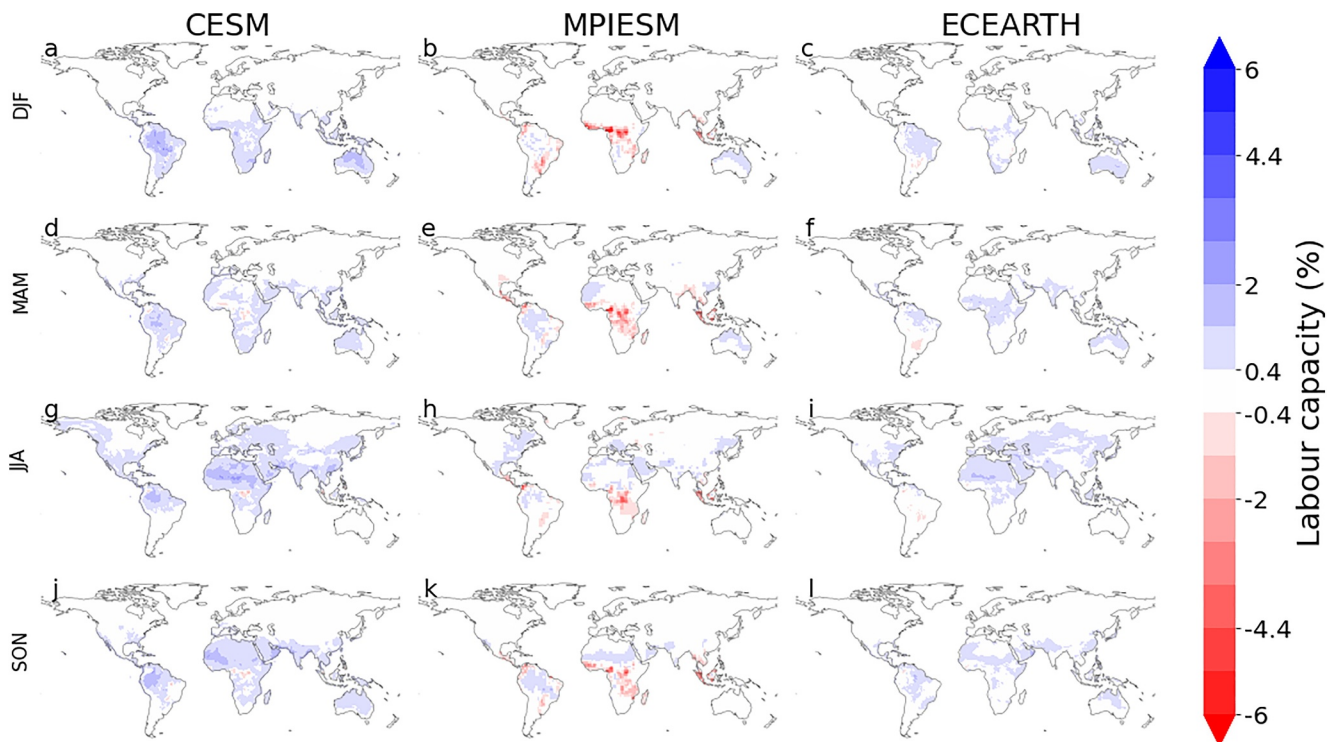


Figure C12. Seasonal averaged labor capacity (%) using the method presented in Havenith et al. (2024) for the three ESMs for the SUST-INEQ case. For CESM, MPI-ESM and EC-EARTH respectively the northern hemisphere spring (MAM) seasonal average (a, b, c), summer (JJA) seasonal average (d, e, f), fall (SON) seasonal average (g, h, i) and the winter (DJF) seasonal average (j, k, l).

Appendix D: Maps of Specific/Relative Humidity, Wind Speed, Incoming Surface Shortwave Radiation

Figure D1

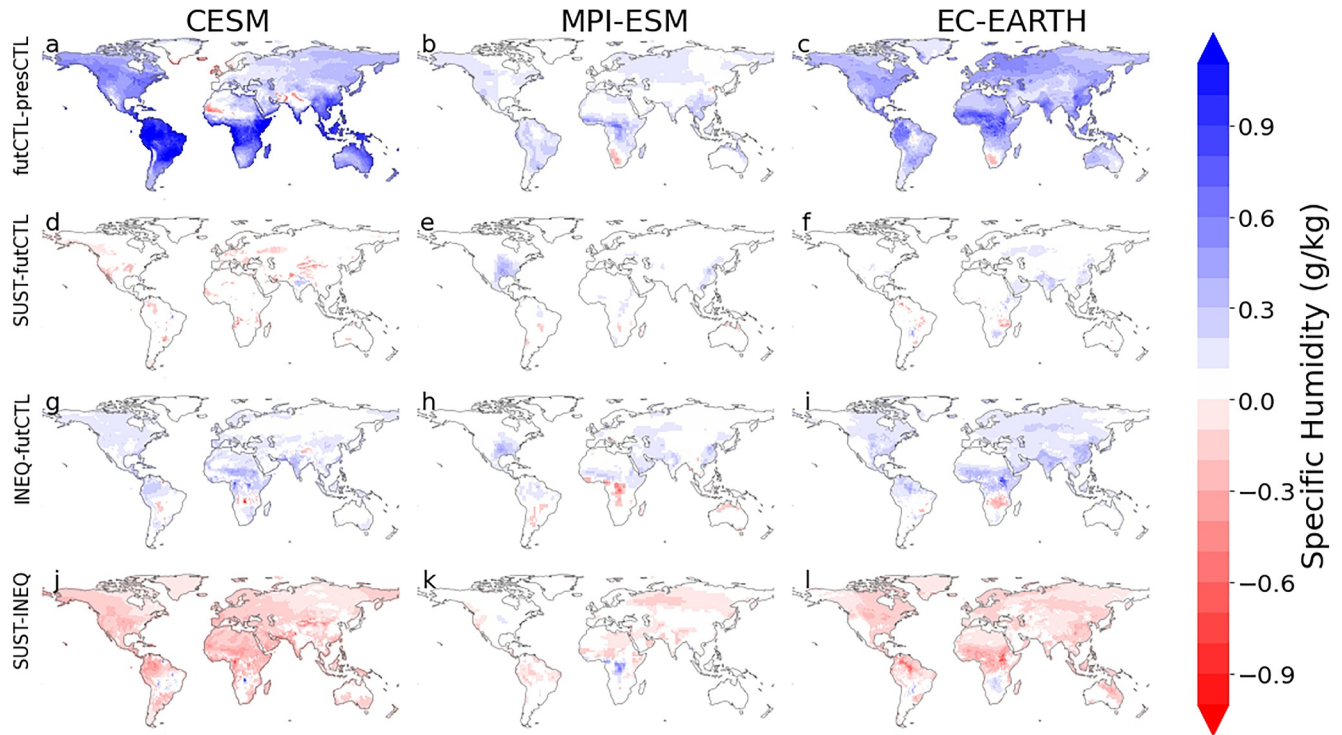


Figure D1. Changes in annual mean near-surface specific humidity (g/kg) by the end of the century (2070–2099) under the RCP1.9 scenario with constant present-day land use for CESM (a), MPI-ESM (b) and EC-EARTH (c), the differences between the sustainability scenario and futCTL for CESM (d), MPI-ESM (e) and EC-EARTH (f), the differences between the inequality scenario and futCTL for CESM (g), MPI-ESM (h) and EC-EARTH (i), and finally the differences between the sustainability and inequality scenario for CESM (g), MPI-ESM (h) and EC-EARTH (i). Only statistically significant changes are shown (0.05 significance level, two-sided Wilcoxon signed rank test of lumped ensemble members and field significance using the false discovery rate test).

Figure D2

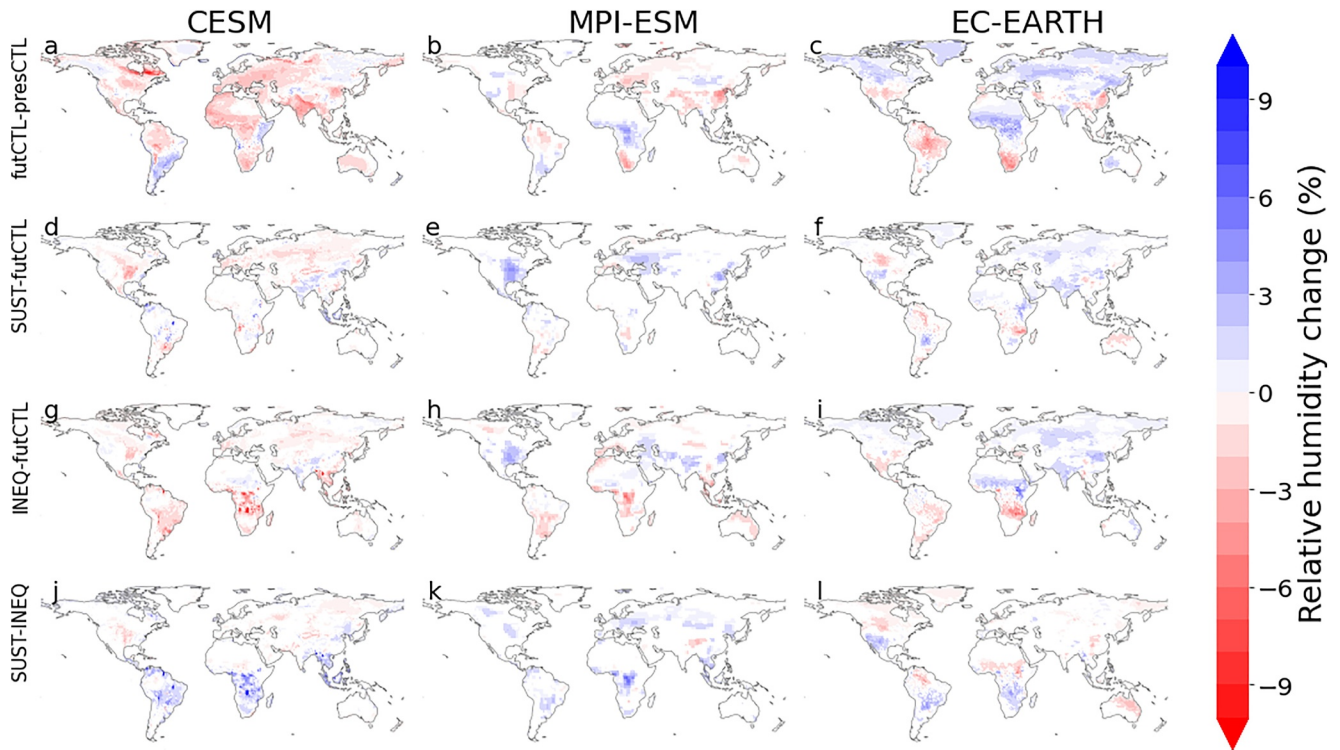


Figure D2. Changes in annual mean near-surface relative humidity (%) by the end of the century (2070–2099) under the RCP1.9 scenario with constant present-day land use for CESM (a), MPI-ESM (b) and EC-EARTH (c), the differences between the sustainability scenario and futCTL for CESM (d), MPI-ESM (e) and EC-EARTH (f), the differences between the inequality scenario and futCTL for CESM (g), MPI-ESM (h) and EC-EARTH (i), and finally the differences between the sustainability and inequality scenario for CESM (g), MPI-ESM (h) and EC-EARTH (i). Only statistically significant changes are shown (0.05 significance level, two-sided Wilcoxon signed rank test of lumped ensemble members and field significance using the false discovery rate test).

Figure D3

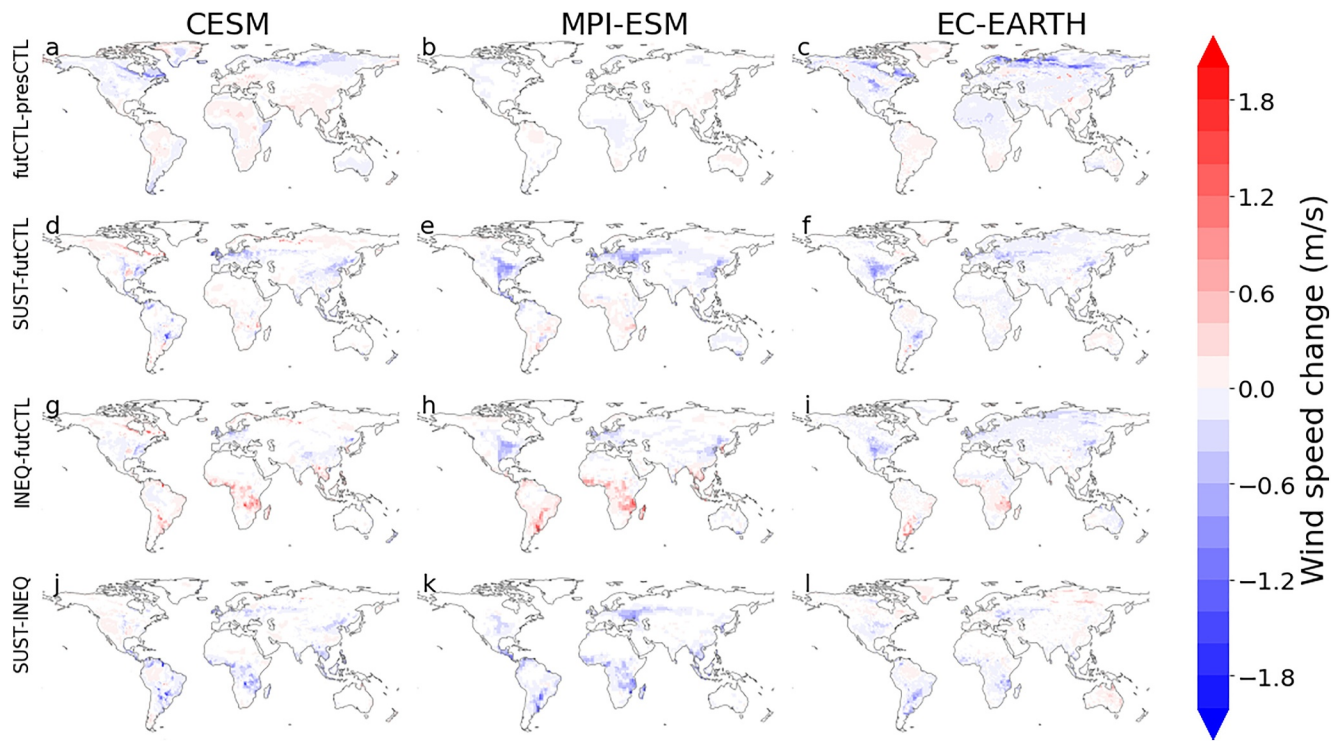


Figure D3. Changes in annual mean near-surface wind speed (m/s) by the end of the century (2070–2099) under the RCP1.9 scenario with constant present-day land use for CESM (a), MPI-ESM (b) and EC-EARTH (c), the differences between the sustainability scenario and futCTL for CESM (d), MPI-ESM (e) and EC-EARTH (f), the differences between the inequality scenario and futCTL for CESM (g), MPI-ESM (h) and EC-EARTH (i), and finally the differences between the sustainability and inequality scenario for CESM (g), MPI-ESM (h) and EC-EARTH (i). Only statistically significant changes are shown (0.05 significance level, two-sided Wilcoxon signed rank test of lumped ensemble members and field significance using the false discovery rate test).

Figure D4

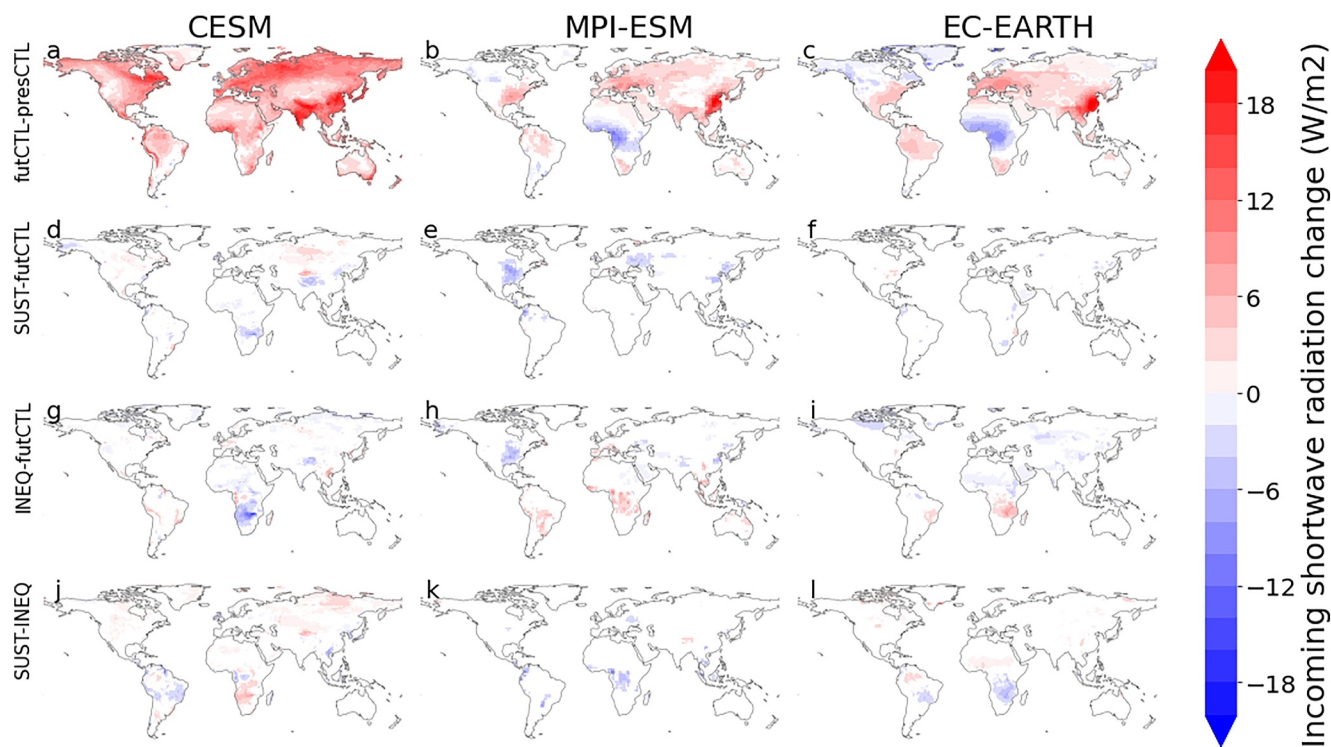


Figure D4. Changes in annual mean incoming surface shortwave radiation (W/m^2) by the end of the century (2070–2099) under the RCP1.9 scenario with constant present-day land use for CESM (a), MPI-ESM (b) and EC-EARTH (c), the differences between the sustainability scenario and futCTL for CESM (d), MPI-ESM (e) and EC-EARTH (f), the differences between the inequality scenario and futCTL for CESM (g), MPI-ESM (h) and EC-EARTH (i), and finally the differences between the sustainability and inequality scenario for CESM (g), MPI-ESM (h) and EC-EARTH (i). Only statistically significant changes are shown (0.05 significance level, two-sided Wilcoxon signed rank test of lumped ensemble members and field significance using the false discovery rate test).

Appendix E: Effects Over Mid Century

Figure E1

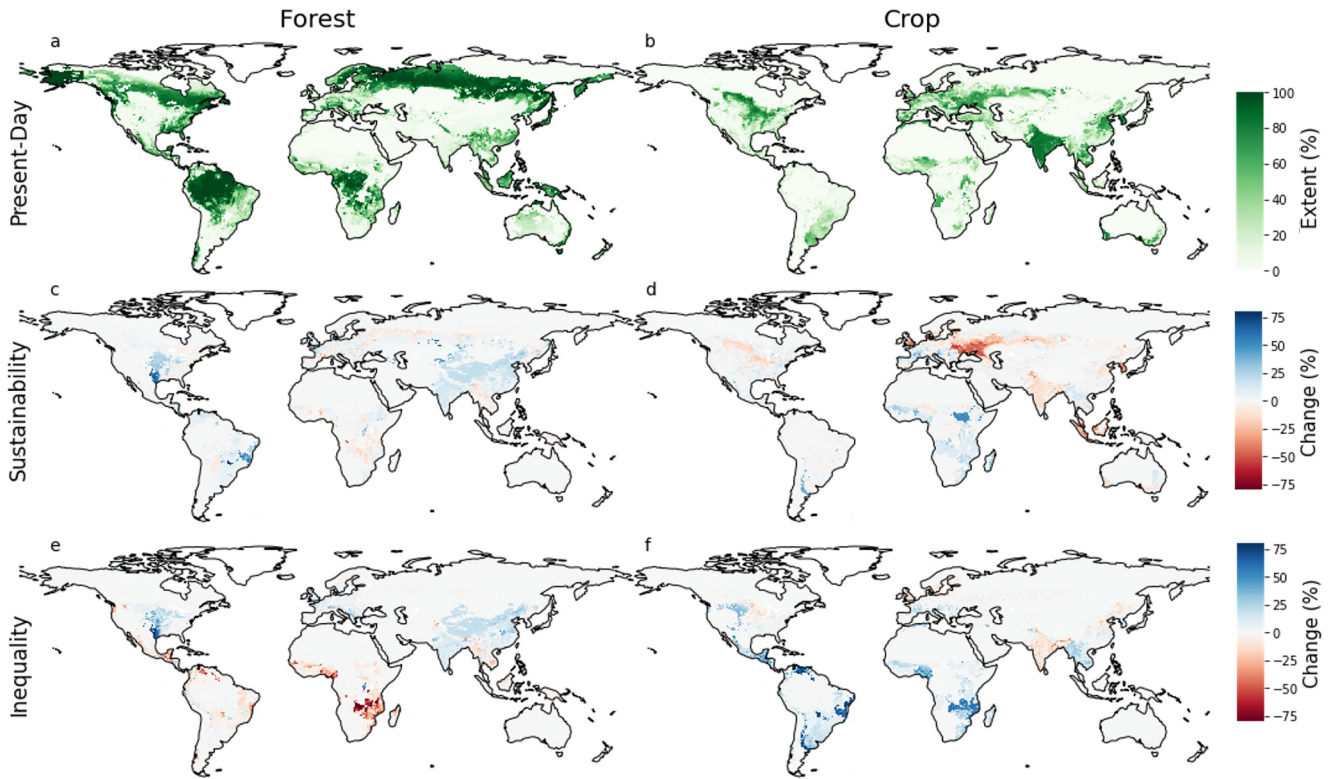


Figure E1. Land-use patterns showing the amount of forest (a) and cropland (b) as a grid cell fraction (%) within the CTL simulations (2014 land-use extent). The change for the sustainability and inequality scenarios respectively are shown for forest (c, d) and cropland (d, f) by the year 2050 (middle of the century).

Figure E2

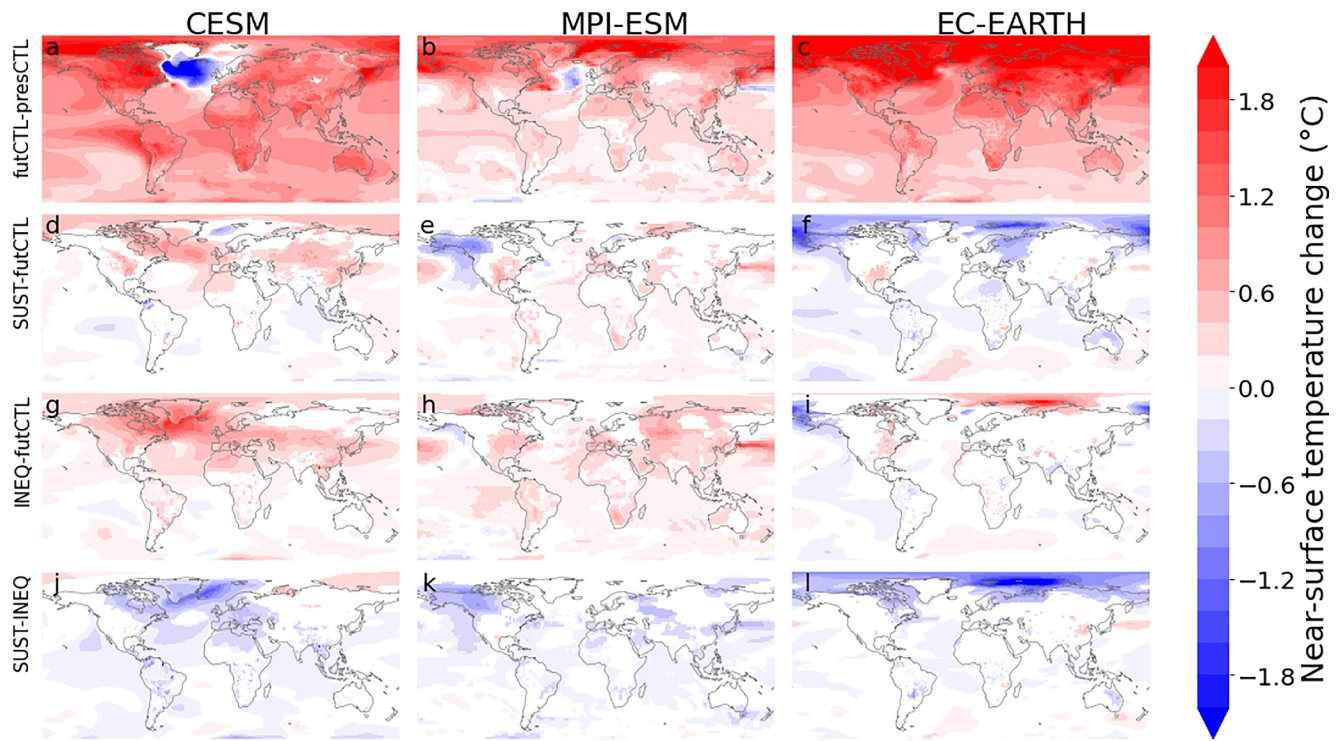


Figure E2. Changes in annual mean near-surface temperature ($^{\circ}\text{C}$) by the middle of the century (2035–2065) under the RCP1.9 scenario with constant present-day land use for CESM (a), MPI-ESM (b) and EC-EARTH (c), the differences between the sustainability scenario and futCTL for CESM (d), MPI-ESM (e) and EC-EARTH (f), the differences between the inequality scenario and futCTL for CESM (g), MPI-ESM (h) and EC-EARTH (i), and finally the differences between the sustainability and inequality scenario for CESM (g), MPI-ESM (h) and EC-EARTH (i). Only statistically significant changes are shown (0.05 significance level, two-sided Wilcoxon signed rank test of lumped ensemble members and field significance using the false discovery rate test).

Table E1

Table E1 <i>Table Summarizing the Differences in Global Mean Temperature (GMT) Between the Simulations Performed With the Three ESMs for the Mid-Century (2035–2065) and End Century (2070–2100)</i>						
GMT	CESM		MPI-ESM		EC-EARTH	
	mid-century	end century	mid-century	end century	mid-century	end century
futCTL-presCTL	1.08	1.05	0.57	0.35	1.20	1.02
INEQ-futCTL	0.23	0.29	0.05	0.17	0.15	0.30
SUST-futCTL	0.12	−0.07	0.05	0.06	−0.05	0.06
SUST-INEQ	−0.10	−0.35	−0.09	−0.10	−0.10	−0.23

Appendix F: ESI

Figure F1

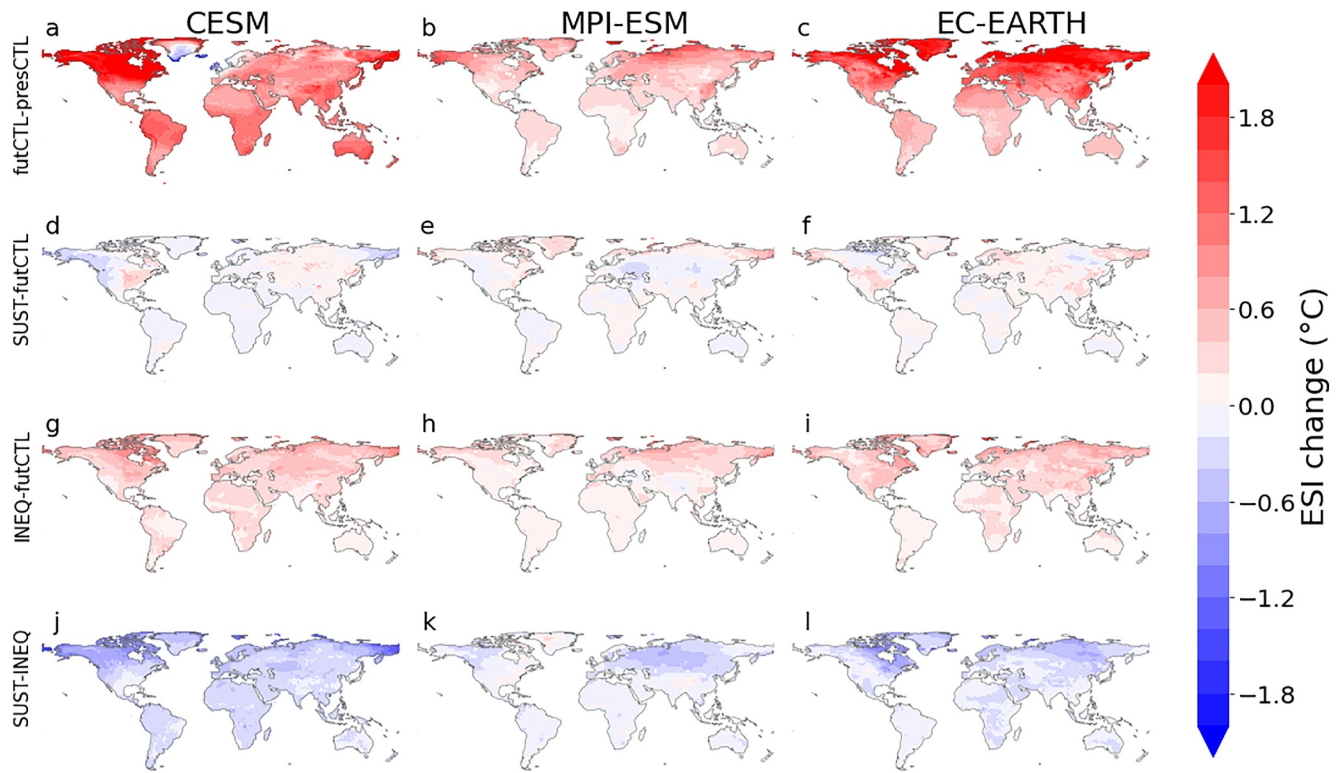


Figure F1. Changes in annual mean environmental stress index ($^{\circ}\text{C}$) by the end of the century (2070–2099) under the RCP1.9 scenario with constant present-day land use for CESM (a), MPI-ESM (b) and EC-EARTH (c), the differences between the sustainability scenario and futCTL for CESM (d), MPI-ESM (e) and EC-EARTH (f), the differences between the inequality scenario and futCTL for CESM (g), MPI-ESM (h) and EC-EARTH (i), and finally the differences between the sustainability and inequality scenario for CESM (g), MPI-ESM (h) and EC-EARTH (i). Only statistically significant changes are shown (0.05 significance level, two-sided Wilcoxon signed rank test of lumped ensemble members and field significance using the false discovery rate test).

Figure F2

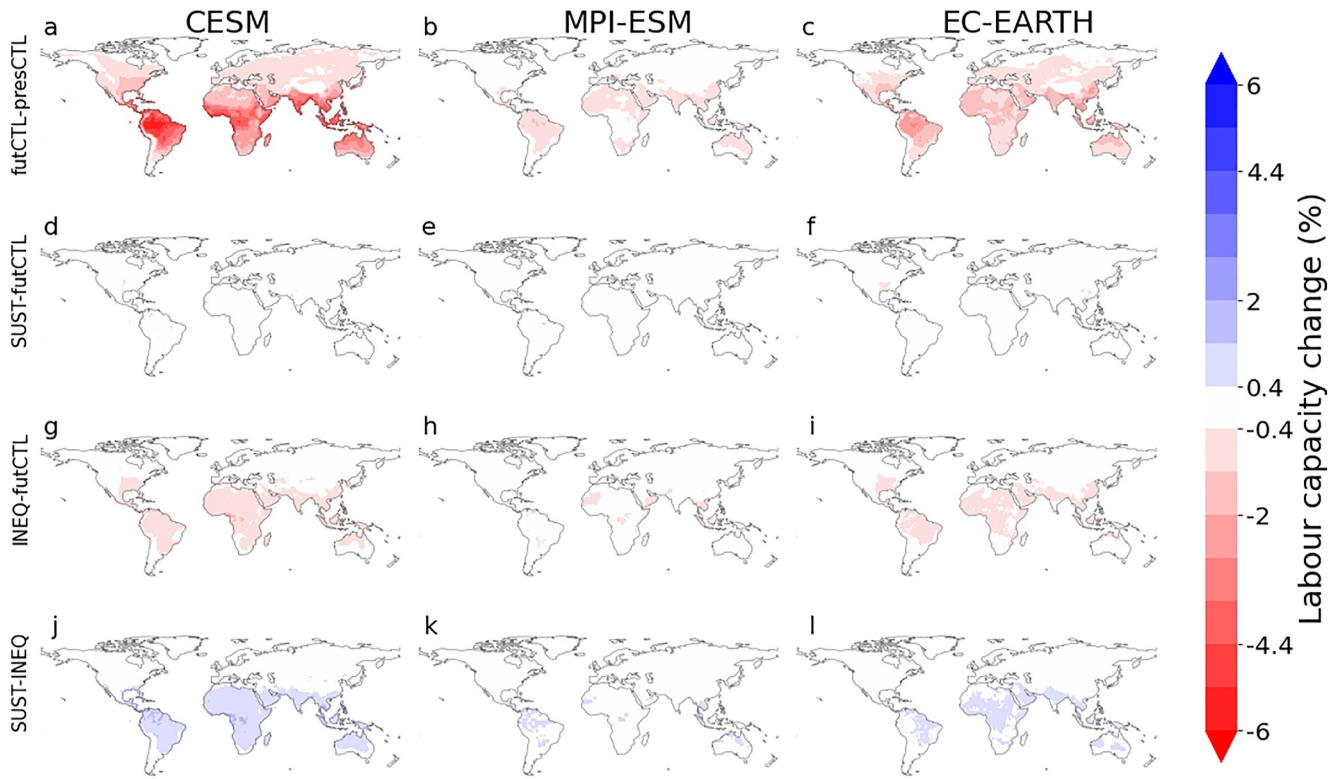


Figure F2. Changes in annual mean labor capacity (%) using the method presented in Havenith et al. (2024) and computed from ESI over a 12hr work day (7a.m.–7p.m.) by the end of the century (2070–2099) under the RCP1.9 scenario with constant present-day land use for CESM (a), MPI-ESM (b) and EC-EARTH (c), the differences between the inequality scenario and futCTL for CESM (d), MPI-ESM (e) and EC-EARTH (f), the differences between the sustainability scenario and futCTL for CESM (g), MPI-ESM (h) and EC-EARTH (i), and finally the differences between the sustainability and inequality scenario for CESM (j), MPI-ESM (k) and EC-EARTH (l).

Appendix G: NIOSH Based Labor Capacity Effects

Figure G1

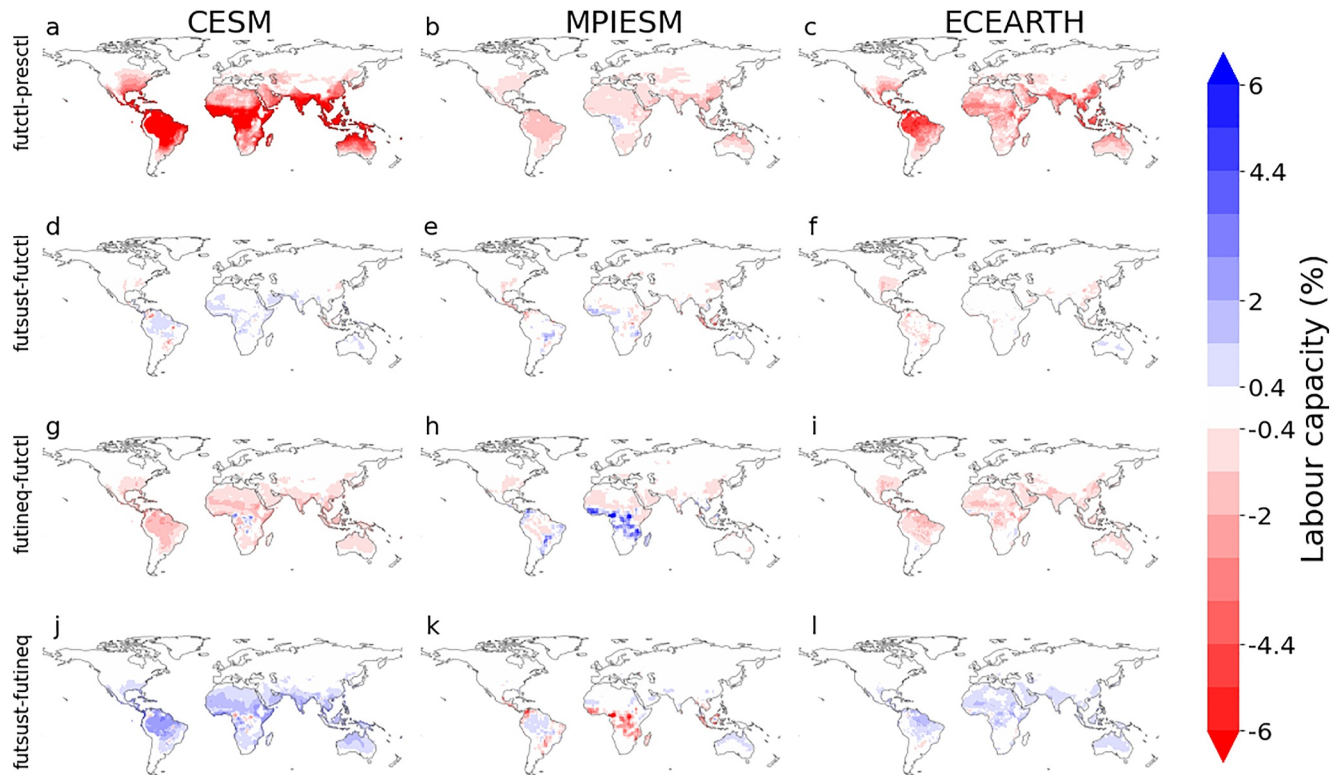


Figure G1. Changes in annual mean labor capacity (%) using the NIOSH recommendations. Values were computed from WBGT over a 12hr work day (7a.m.–7p.m.) by the end of the century (2070–2099) between the futCTL and presCTL scenarios, the sustainability and futCTL scenarios, the inequality and futCTL scenarios, and the sustainability and inequality scenarios, for CESM (a, d, g, j), MPI-ESM (b, e, h, k) and EC-EARTH (c, f, i, l), respectively.

Acknowledgments

This work was funded by the LAMACLIMA (“LAnd MAnagement for CLimate Mitigation and Adaptation”) project which is part of AXIS, an ERA-NET initiated by JPI Climate, and funded by DLR/BMBF (DE, Grant 01LS1905A), NWO (NL, Grant 438.19.904), RCN (NO, Grant 300478) and BELSPO (BE, Grant B2/181/P1) with co-funding by the European Union (Grant 776608). The computational resources and services used in this work for the simulations and storage of CESM data were provided by the VSC (Flemish Supercomputer Center), funded by the Research Foundation - Flanders (FWO) and the Flemish Government–department EWI. For the storage and computation of the simulations for MPI-ESM, this work used resources of the Deutsches Klimarechenzentrum (DKRZ) granted by its Scientific Steering Committee (WLA) under project ID bm1147. All the simulations from EC-EARTH were carried out on European Center for Medium-Range Weather Forecast (ECMWF) platforms. The contributions from LC and GCH

Data Availability Statement

CESM is an open source model which can be freely downloaded here (https://www.cesm.ucar.edu/models/cesm2/release_download.html). The scripts used for this analysis can be accessed through GitHub (De Hertog, 2024b). The postprocessed ESM data used for the figures in this manuscript is available through Doku (De Hertog, 2024a). The raw simulation data of the ESMs used in this paper (more than 130 TB for CESM only) will be made available through the Deutsches Klimarechenzentrum (DKRZ), for those interested in using these data please contact the authors.

References

Arias, P., Bellouin, N., Coppola, E., Jones, R., Krinner, G., Marotzke, J., & Zickfeld, K. (2021). 2021: Technical summary. In P. Zhai, A. Pirani, S. L. Connors, & C. Péan (Eds.), *Climate change 2021: The physical science basis. Contribution of working group I to the sixth assessment report of the intergovernmental panel on climate change Masson-Delmotte, V. S.* Cambridge University Press(August). 150 Retrieved from https://www.ipcc.ch/report/ar6/wg1/downloads/report/IPCC_AR6_WGL_TS.pdf

Bacmeister, J. T., Hannay, C., Medeiros, B., Gettelman, A., Neale, R., Fredriksen, H.-B., et al. (2020). CO₂ increase experiments using the CESM: Relationship to climate sensitivity and comparison of CESM1 to CESM2. *Journal of Advances in Modeling Earth Systems*, 12(11), e2020MS002120. <https://doi.org/10.1029/2020ms002120>

Beusch, L., Gudmundsson, L., & Seneviratne, S. I. (2020). Crossbreeding CMIP6 earth system models with an emulator for regionally optimized land temperature projections. *Geophysical Research Letters*, 47(15), e2019GL086812. <https://doi.org/10.1029/2019gl086812>

Boisier, J. P., De Noblet-Ducoudré, N., Pitman, A. J., Cruz, F. T., Delire, C., Van Den Hurk, B. J., et al. (2012). Attributing the impacts of land-cover changes in temperate regions on surface temperature and heat fluxes to specific causes: Results from the first LUCID set of simulations. *Journal of Geophysical Research*, 117(12), 1–16. <https://doi.org/10.1029/2011JD017106>

Boysen, L. R., Brovkin, V., Arora, V. K., Cadule, P., de Noblet-Ducoudré, N., Kato, E., et al. (2014). Global and regional effects of land-use change on climate in 21st century simulations with interactive carbon cycle. *Earth System Dynamics*, 5(2), 309–319. <https://doi.org/10.5194/esd-5-309-2014>

were funded by the NASA Carbon Monitoring System program (80NSSC21K1059). WT received funding from the European Research Council (ERC) under the European Union's Horizon Framework research and innovation programme (grant agreement No 101076909; "LACRIMA" project). SDH acknowledges funding by BELSPO (B2/223/P1/DAMOCO).

- Boysen, L. R., Brovkin, V., Pongratz, J., Lawrence, D. M., Lawrence, P., Vuichard, N., et al. (2020). Global climate response to idealized deforestation in CMIP6 models. *Biogeosciences*, *17*(22), 5615–5638. <https://doi.org/10.5194/bg-17-5615-2020>
- Brimicombe, C., Di Napoli, C., Quintino, T., Pappenberger, F., Cornforth, R., & Cloke, H. L. (2022). Thermofeel: A python thermal comfort indices library. *SoftwareX*, *18*, 101005. <https://doi.org/10.1016/j.softx.2022.101005>
- Brovkin, V., Boysen, L., Arora, V. K., Boisier, J., Cadule, P., Chini, L., et al. (2013). Effect of anthropogenic land-use and land-cover changes on climate and land carbon storage in CMIP5 projections for the twenty-first century. *Journal of Climate*, *26*(18), 6859–6881. <https://doi.org/10.1175/jcli-d-12-00623.1>
- Budd, G. M. (2008). Wet-Bulb Globe Temperature (WBGT)—Its history and its limitations. *Journal of Science and Medicine in Sport*, *11*(1), 20–32. <https://doi.org/10.1016/j.jsams.2007.07.003>
- Buzan, J., Oleson, K., & Huber, M. (2015). Implementation and comparison of a suite of heat stress metrics within the community land model version 4.5. *Geoscientific Model Development*, *8*(2), 151–170. <https://doi.org/10.5194/gmd-8-151-2015>
- Buzan, J. R., & Huber, M. (2020). Moist heat stress on a hotter earth. *Annual Review of Earth and Planetary Sciences*, *48*(1), 623–655. <https://doi.org/10.1146/annurev-earth-053018-060100>
- Chakraborty, T., Qian, Y., Li, J., Leung, L., & Sarangi, C. (2024). Irrigation tends to reduce daytime urban heat stress in north America. *Nature*, under review. <https://doi.org/10.21203/rs.3.rs-4017285/v1>
- Chausson, A., Turner, B., Seddon, D., Chabaneix, N., Girardin, C. A., Kapos, V., et al. (2020). Mapping the effectiveness of nature-based solutions for climate change adaptation. *Global Change Biology*, *26*(11), 6134–6155. <https://doi.org/10.1111/gcb.15310>
- Danabasoglu, G., Lamarque, J. F., Bacmeister, J., Bailey, D. A., DuVivier, A. K., Edwards, J., et al. (2020). The Community Earth System Model Version 2 (CESM2). *Journal of Advances in Modeling Earth Systems*, *12*(2), 1–35. <https://doi.org/10.1029/2019MS001916>
- Davin, E. L., & de Noblet-Ducoudré, N. (2010). Climatic impact of global-scale Deforestation: Radiative versus nonradiative processes. *Journal of Climate*, *23*(1), 97–112. <https://doi.org/10.1175/2009JCLI3102.1>
- Davin, E. L., Seneviratne, S. I., Ciais, P., Ollio, A., & Wang, T. (2014). Preferential cooling of hot extremes from cropland albedo management. *Proceedings of the National Academy of Sciences*, *111*(27), 9757–9761. <https://doi.org/10.1073/pnas.1317323111>
- De Hertog, S. J. (2024a). Data underlying submission of de Hertog et al. 2024 to earth's future (version 2) [Dataset]. *World Data Center for Climate (WDCC) at DKRZ*. Retrieved from <https://hdl.handle.net/21.14106/e1c562742f380d4420cfe93672e27a9edba24a>
- De Hertog, S. J. (2024b). Scripts underlying submission of de Hertog et al. 2024 to earth's future [Software]. *Zenodo*. <https://doi.org/10.5281/zenodo.13852311>
- De Hertog, S. J., Havermann, F., Vanderkelen, I., Guo, S., Luo, F., Manola, I., et al. (2023). The biogeophysical effects of idealized land cover and land management changes in Earth system models. *Earth System Dynamics*, *14*(3), 629–667. <https://doi.org/10.5194/egusphere-2023-253>
- De Hertog, S. J., Lopez-Fabara, C. E., van der Ent, R., Keune, J., Miralles, A. K., Portmann, R., et al. (2024). Effects of idealized land cover and land management changes on the atmospheric water cycle. *Earth System Dynamics*, *15*(2), 265–291. <https://doi.org/10.5194/esd-15-265-2024>
- De Lima, C. Z., Buzan, J. R., Moore, F. C., Baldos, U. L. C., Huber, M., & Hertel, T. W. (2021). Heat stress on agricultural workers exacerbates crop impacts of climate change. *Environmental Research Letters*, *16*(4), 044020. <https://doi.org/10.1088/1748-9326/abeb9f>
- De Noblet-Ducoudré, N., Boisier, J. P., Pitman, A., Bonan, G. B., Brovkin, V., Cruz, F., et al. (2012). Determining robust impacts of land-use-induced land cover changes on surface climate over North America and Eurasia: Results from the first set of LUCID experiments. *Journal of Climate*, *25*(9), 3261–3281. <https://doi.org/10.1175/JCLI-D-11-00338.1>
- Döscher, R., Acosta, M., Alessandri, A., Anthoni, P., Arsouze, T., Bergman, T., et al. (2022). The EC-Earth3 earth system model for the coupled model intercomparison project 6. *Geoscientific Model Development*, *15*(7), 2973–3020. <https://doi.org/10.5194/gmd-15-2973-2022>
- Dunne, J. P., Stouffer, R. J., & John, J. G. (2013). Reductions in labour capacity from heat stress under climate warming. *Nature Climate Change*, *3*(6), 563–566. <https://doi.org/10.1038/nclimate1827>
- Duveiller, G., Caporaso, L., Abad-Viñas, R., Perugini, L., Grassi, G., Arneth, A., & Cescatti, A. (2020). Local biophysical effects of land use and land cover change: Towards an assessment tool for policy makers. *Land Use Policy*, *91*(August 2018), 104382. <https://doi.org/10.1016/j.landusepol.2019.104382>
- Duveiller, G., Hooker, J., & Cescatti, A. (2018). The mark of vegetation change on Earth's surface energy balance. *Nature Communications*, *9*(9), 679. <https://doi.org/10.1038/s41467-017-02810-8>
- Eyring, V., Bony, S., Meehl, G. A., Senior, C. A., Stevens, B., Stouffer, R. J., & Taylor, K. E. (2016). Overview of the coupled model intercomparison project phase 6 (CMIP6) experimental design and organization. *Geoscientific Model Development*, *9*(5), 1937–1958. <https://doi.org/10.5194/gmd-9-1937-2016>
- Fatima, S. H., Rothmore, P., Giles, L. C., Varghese, B. M., & Bi, P. (2021). Extreme heat and occupational injuries in different climate zones: A systematic review and meta-analysis of epidemiological evidence. *Environment International*, *148*, 106384. <https://doi.org/10.1016/j.envint.2021.106384>
- Gettelman, A., Hannay, C., Bacmeister, J. T., Neale, R. B., Pendergrass, A., Danabasoglu, G., et al. (2019). High climate sensitivity in the Community Earth System Model Version 2 (CESM2). *Geophysical Research Letters*, *46*(14), 8329–8337. <https://doi.org/10.1029/2019gl083978>
- Havenith, G., Smallcombe, J. W., Hodder, S., Jay, O., & Foster, J. (2024). Comparing efficacy of different climate indices for predicting Labor loss, body temperature, and thermal perception in a wide variety of warm and hot climates. *Journal of Applied Physiology*, *137*(2), 312–328. <https://doi.org/10.1152/jappphysiol.00613.2023>
- Hirsch, A. L., Guillod, B. P., Seneviratne, S. I., Beyerle, U., Boysen, L. R., Brovkin, V., et al. (2018). Biogeophysical impacts of land-use change on climate extremes in low-emission scenarios: Results from happi-land. *Earth's Future*, *6*(3), 396–409. <https://doi.org/10.1002/2017ef000744>
- Humpenöder, F., Popp, A., Schleussner, C.-F., Orlov, A., Windisch, M. G., Menke, I., et al. (2022). Overcoming global inequality is critical for land-based mitigation in line with the Paris agreement. *Nature Communications*, *13*(1), 7453. <https://doi.org/10.1038/s41467-022-35114-7>
- Hurt, G. C., Chini, L., Sahajpal, R., Frolking, S., Bodirsky, B. L., Calvin, K., et al. (2020). Harmonization of global land use change and management for the period 850–2100 (LUH2) for CMIP6. *Geoscientific Model Development*, *13*(11), 5425–5464. <https://doi.org/10.5194/gmd-13-5425-2020>
- Ioannou, L. G., Mantzios, K., Tsoutsoubi, L., Notley, S. R., Dinas, P. C., Brearley, M., et al. (2022a). Indicators to assess physiological heat strain—part 1: Systematic review. *Temperature*, *9*(3), 227–262. <https://doi.org/10.1080/23328940.2022.2037376>
- Ioannou, L. G., Tsoutsoubi, L., Mantzios, K., Vliora, M., Nintou, E., Pii, J. F., et al. (2022b). Indicators to assess physiological heat strain—part 3: Multi-country field evaluation and consensus recommendations. *Temperature*, *9*(3), 274–291. <https://doi.org/10.1080/23328940.2022.2044739>
- IPCC. (2021). [Book]. In V. Masson-Delmotte, et al. (Eds.), *Climate change 2021: The physical science basis. Contribution of working group I to the sixth assessment report of the intergovernmental panel on climate change*. Cambridge University Press. <https://doi.org/10.1017/9781009157896>

- IPCC. (2022). In P. R. Shukla, J. Skea, R. Slade, A. Al Khouradajie, R. van Diemen, D. McCollum, et al. (Eds.), *Climate change 2022: Mitigation of climate change. Contribution of working group III to the sixth assessment report of the intergovernmental panel on climate change*. IPCC.
- Jia, G., Shevliakova, E., Artaxo, P., De Noblet-Ducoudré, N., Houghton, R., House, J., et al. (2019). Land–climate interactions. In P. R. Shukla, J. Skea, E. Calvo Buendia, V. Masson-Delmotte, H.-O. Pörtner, D. C. Roberts, et al. (Eds.), *Climate change and land: An IPCC special report on climate change, desertification, land degradation, sustainable land management, food security, and greenhouse gas fluxes in terrestrial ecosystems*. Cambridge University Press August.
- Kamal, A. M., Faruki Fahim, A. K., & Shahid, S. (2024). Simplified equations for wet bulb globe temperature estimation in Bangladesh. *International Journal of Climatology*, *44*(5), 1636–1653. <https://doi.org/10.1002/joc.8402>
- Kjellstrom, T., Freyberg, C., Lemke, B., Otto, M., & Briggs, D. (2018). Estimating population heat exposure and impacts on working people in conjunction with climate change. *International Journal of Biometeorology*, *62*(3), 291–306. <https://doi.org/10.1007/s00484-017-1407-0>
- Kjellstrom, T., Holmer, I., & Lemke, B. (2009). Workplace heat stress, health and productivity—an increasing challenge for low and middle-income countries during climate change. *Global Health Action*, *2*(1), 2047. <https://doi.org/10.3402/gha.v2i0.2047>
- Kong, Q., & Huber, M. (2022). Explicit calculations of wet-bulb globe temperature compared with approximations and why it matters for Labor productivity. *Earth's Future*, *10*(3), e2021EF002334. <https://doi.org/10.1029/2021ef002334>
- Kong, Q., & Huber, M. (2024a). *A linear sensitivity framework to understand the drivers of the wet-bulb globe temperature changes*. Researchsquare.
- Kong, Q., & Huber, M. (2024b). A new, zero-iteration analytic implementation of wet-bulb globe temperature: Development, validation and comparison with other methods. *Authorea Preprints*, *8*(10). <https://doi.org/10.1029/2024gh001068>
- Lawrence, D. M., Hurr, G. C., Arneth, A., Brovkin, V., Calvin, K. V., Jones, A. D., et al. (2016). The Land Use Model Intercomparison Project (LUMIP) contribution to CMIP6: Rationale and experimental design. *Geoscientific Model Development*, *9*, 2973–2998. <https://doi.org/10.5194/gmd-9-2973-2016>
- Lejeune, Q., Davin, E. L., Gudmundsson, L., Winckler, J., & Seneviratne, S. I. (2018). Historical deforestation locally increased the intensity of hot days in northern mid-latitudes. *Nature Climate Change*, *8*(5), 386–390. <https://doi.org/10.1038/s41558-018-0131-z>
- Lemke, B., & Kjellstrom, T. (2012). Calculating workplace WBGT from meteorological data: A tool for climate change assessment. *Industrial Health*, *50*(4), 267–278. <https://doi.org/10.2486/indhealth.ms1352>
- Liljegren, J. C., Carhart, R. A., Lawday, P., Tschopp, S., & Sharp, R. (2008). Modeling the wet bulb globe temperature using standard meteorological measurements. *Journal of Occupational and Environmental Hygiene*, *5*(10), 645–655. <https://doi.org/10.1080/15459620802310770>
- Lorenz, R., Pitman, A., & Sisson, S. A. (2016). Does amazonian deforestation cause global effects; can we be sure? *Journal of Geophysical Research: Atmospheres*, *121*(10), 5567–5584. <https://doi.org/10.1002/2015jd024357>
- Mauritsen, T., Bader, J., Becker, T., Behrens, J., Bittner, M., Brokopf, R., et al. (2019). Developments in the MPI-M earth system model version 1.2 (MPI-ESM1.2) and its response to increasing CO₂. *Journal of Advances in Modeling Earth Systems*, *11*(4), 998–1038. <https://doi.org/10.1029/2018MS001400>
- Mauritsen, T., & Roeckner, E. (2020). Tuning the Mpi-Esm1. 2 Global climate model to improve the match with instrumental record warming by lowering its climate sensitivity. *Journal of Advances in Modeling Earth Systems*, *12*(5), e2019MS002037. <https://doi.org/10.1029/2019ms002037>
- Meehl, G. A., Senior, C. A., Eyring, V., Flato, G., Lamarque, J.-F., Stouffer, R. J., et al. (2020). Context for interpreting equilibrium climate sensitivity and transient climate response from the CMIP6 earth system models. *Science Advances*, *6*(26), eaba1981. <https://doi.org/10.1126/sciadv.aba1981>
- Meier, R., Schwaab, J., Seneviratne, S. I., Sprenger, M., Lewis, E., & Davin, E. L. (2021). Empirical estimate of forestation-induced precipitation changes in Europe. *Nature Geoscience*, *14*(7), 473–478. <https://doi.org/10.1038/s41561-021-00773-6>
- Mishra, V., Ambika, A. K., Asoka, A., Aadhar, S., Buzan, J., Kumar, R., & Huber, M. (2020). Moist heat stress extremes in India enhanced by irrigation. *Nature Geoscience*, *13*(11), 722–728. <https://doi.org/10.1038/s41561-020-00650-8>
- Mora, C., Dousset, B., Caldwell, I. R., Powell, F. E., Geronimo, R. C., Bielecki, C. R., et al. (2017). Global risk of deadly heat. *Nature Climate Change*, *7*(7), 501–506. <https://doi.org/10.1038/nclimate3322>
- Morice, C. P., Kennedy, J. J., Rayner, N. A., Winn, J., Hogan, E., Killick, R., et al. (2021). An updated assessment of near-surface temperature change from 1850: The Hadcrut5 data set. *Journal of Geophysical Research: Atmospheres*, *126*(3), e2019JD032361. <https://doi.org/10.1029/2019jd032361>
- Nath, S., Gudmundsson, L., Schwaab, J., Duveiller, G., De Hertog, S. J., Guo, S., et al. (2023). Timber v0. 1: A conceptual framework for emulating temperature responses to tree cover change. *Geoscientific Model Development*, *16*(14), 4283–4313. <https://doi.org/10.5194/gmd-16-4283-2023>
- Nath, S., Lejeune, Q., Beusch, L., Seneviratne, S. I., & Schleussner, C.-F. (2022). Mesmer-m: An earth system model emulator for spatially resolved monthly temperature. *Earth System Dynamics*, *13*(2), 851–877. <https://doi.org/10.5194/esd-13-851-2022>
- NIOSH. (1986). *Criteria for a recommended standard: Occupational exposure to hot environments*. National Institute for Occupational Safety and Health.
- Oleson, K. W., Monaghan, A., Wilhelmi, O., Barlage, M., Brunzell, N., Feddema, J., et al. (2015). Interactions between urbanization, heat stress, and climate change. *Climatic Change*, *129*(3–4), 525–541. <https://doi.org/10.1007/s10584-013-0936-8>
- Orlov, A., Aunan, K., Mistry, M. N., Lejeune, Q., Pongratz, J., Thiery, W., et al. (2023a). Neglected implications of land-use and land-cover changes on the climate-health nexus. *Environmental Research Letters*, *18*(6), 061005. <https://doi.org/10.1088/1748-9326/acd799>
- Orlov, A., Daloz, A. S., Sillmann, J., Thiery, W., Douzal, C., Lejeune, Q., & Schleussner, C. (2021). Global economic responses to heat stress impacts on worker productivity in crop production. *Economics of Disasters and Climate Change*, *5*(3), 367–390. <https://doi.org/10.1007/s41885-021-00091-6>
- Orlov, A., De Hertog, S., Havermann, F., Guo, S., Luo, F., Manola, I., et al. (2023b). Changes in land cover and management affect heat stress and labor capacity. *Earth's Future*, *11*(3), e2022EF002909. <https://doi.org/10.1029/2022ef002909>
- Orlov, A., De Hertog, S. J., Havermann, F., Guo, S., Manola, I., Lejeune, Q., et al. (2024a). Impacts of land-use and land-cover changes on temperature-related mortality. *Environmental Epidemiology*, *8*(6), e337. <https://doi.org/10.1097/ee9.0000000000000337>
- Orlov, A., Jägermeyr, J., Müller, C., Daloz, A. S., Zabel, F., Minoli, S., et al. (2024b). Human heat stress could offset potential economic benefits of CO₂ fertilization in crop production under a high-emissions scenario. *One Earth*, *7*(7), 1250–1265. <https://doi.org/10.1016/j.oneear.2024.06.012>
- Orlov, A., Sillmann, J., Aunan, K., Kjellstrom, T., & Aaheim, A. (2020). Economic costs of heat-induced reductions in worker productivity due to global warming. *Global Environmental Change*, *63*, 102087. <https://doi.org/10.1016/j.gloenvcha.2020.102087>

- Pitman, A. J., De Noblet-Ducoudré, N., Cruz, F. T., Davin, E. L., Bonan, G. B., Brovkin, V., et al. (2009). Uncertainties in climate responses to past land cover change: First results from the LUCID intercomparison study. *Geophysical Research Letters*, *36*(14), 1–6. <https://doi.org/10.1029/2009GL039076>
- Pongratz, J., Reick, C., Raddatz, T., & Claussen, M. (2010). Biogeophysical versus biogeochemical climate response to historical anthropogenic land cover change. *Geophysical Research Letters*, *37*(8). <https://doi.org/10.1029/2010gl043010>
- Pongratz, J., Schwingshackl, C., Bultan, S., Obermeier, W., Havermann, F., & Guo, S. (2021). Land use effects on climate: Current State, recent progress, and emerging topics. *Current Climate Change Reports*, *7*(4), 0123456789–123457120. <https://doi.org/10.1007/s40641-021-00178-y>
- Portmann, R., Beyerle, U., Davin, E., Fischer, E. M., De Hertog, S., & Schemm, S. (2022). Global forestation and deforestation affect remote climate via adjusted atmosphere and ocean circulation. *Nature Communications*, *13*(1), 1–11. <https://doi.org/10.1038/s41467-022-33279-9>
- Riahi, K., Van Vuuren, D. P., Kriegler, E., Edmonds, J., O'Neill, B. C., Fujimori, S., et al. (2017). The shared socioeconomic pathways and their energy, land use, and greenhouse gas emissions implications: An overview. *Global Environmental Change*, *42*, 153–168. <https://doi.org/10.1016/j.gloenvcha.2016.05.009>
- Roe, S., Streck, C., Obersteiner, M., Frank, S., Griscom, B., Drouet, L., et al. (2019). Contribution of the land sector to a 1.5°C world. *Nature Climate Change*, *9*(11), 817–828. <https://doi.org/10.1038/s41558-019-0591-9>
- Rogelj, J., Shindell, D., Jiang, K., Fifita, S., Forster, P., Ginzburg, V., et al. (2018). *Mitigation pathways compatible with 1.5c in the context of sustainable development*. (pp. 93–174). IPCC.
- Seneviratne, S. I., Wartenburger, R., Guillod, B. P., Hirsch, A. L., Vogel, M. M., Brovkin, V., et al. (2018). Climate extremes, land–climate feedbacks and land-use forcing at 1.5c. *Philosophical Transactions of the Royal Society A: Mathematical, Physical & Engineering Sciences*, *376*(2119), 20160450. <https://doi.org/10.1098/rsta.2016.0450>
- Soergel, B., Kriegler, E., Weindl, I., Rauner, S., Dirmaichner, A., Ruhe, C., et al. (2021). A sustainable development pathway for climate action within the un 2030 agenda. *Nature Climate Change*, *11*(8), 656–664. <https://doi.org/10.1038/s41558-021-01098-3>
- Thiery, W., Davin, E. L., Lawrence, D. M., Hirsch, A. L., Hauser, M., & Seneviratne, S. I. (2017). Present-day irrigation mitigates heat extremes. *Journal of Geophysical Research*, *122*(3), 1403–1422. <https://doi.org/10.1002/2016JD025740>
- Thiery, W., Visser, A. J., Fischer, E. M., Hauser, M., Hirsch, A. L., Lawrence, D. M., et al. (2020). Warming of hot extremes alleviated by expanding irrigation. *Nature Communications*, *11*(1), 1–7. <https://doi.org/10.1038/s41467-019-14075-4>
- UNFCCC. (2015). Adoption of the Paris agreement [report No. FCCC/CP/2015/L.9/Rev.1]. *United Nations Framework Convention on Climate Change (UNFCCC)*. Retrieved from <http://unfccc.int/resource/docs/2015/cop21/eng/l09r01.pdf>
- Vanderkelen, I., Lipzig, N. P. M., Sacks, W. J., Lawrence, D. M., Clark, M. P., Mizukami, N., et al. (2021). Simulating the impact of global reservoir expansion on the present-day climate. *Journal of Geophysical Research: Atmospheres*, *126*(16). <https://doi.org/10.1029/2020jd034485>
- Wilks, D. (2006). On “field significance” and the false discovery rate. *Journal of Applied Meteorology and Climatology*, *45*(9), 1181–1189. <https://doi.org/10.1175/jam2404.1>
- Winckler, J., Lejeune, Q., Reick, C. H., & Pongratz, J. (2019). Nonlocal effects dominate the global mean surface temperature response to the biogeophysical effects of deforestation. *Geophysical Research Letters*, *46*(2), 745–755. <https://doi.org/10.1029/2018gl080211>
- Winckler, J., Reick, C. H., & Pongratz, J. (2017). Robust identification of local biogeophysical effects of land-cover change in a global climate model. *Journal of Climate*, *30*(3), 1159–1176. <https://doi.org/10.1175/jcli-d-16-0067.1>
- Wouters, H., De Ridder, K., Poelmans, L., Willems, P., Brouwers, J., Hosseinzadehtalaei, P., et al. (2017). Heat stress increase under climate change twice as large in cities as in rural areas: A study for a densely populated midlatitude maritime region. *Geophysical Research Letters*, *44*(17), 8997–9007. <https://doi.org/10.1002/2017gl074889>
- Wyser, K., van Noije, T., Yang, S., von Hardenberg, J., O'Donnell, D., & Döscher, R. (2020). On the increased climate sensitivity in the EC-Earth model from CMIP5 to CMIP6. *Geoscientific Model Development*, *13*(9), 3465–3474. <https://doi.org/10.5194/gmd-13-3465-2020>
- Yaglou, C., & Minard, D. (1957). Control of heat casualties at military training centers. *Archives of industrial health*, *16*(4), 302–316.
- Yao, Y., Schanke Aas, K., Buzan, J., Colin, J., Cook, B., Costantini, M., et al. (2024). Impacts of irrigation expansion on moist-heat stress: First results from IRRMIP. *Nature Communications*, under review. <https://doi.org/10.21203/rs.3.rs-4835411/v1>
- Yao, Y., Vanderkelen, I., Lombardozi, D., Swenson, S., Lawrence, D., Jägermeyr, J., et al. (2022). Implementation and evaluation of irrigation techniques in the community land model. *Journal of Advances in Modeling Earth Systems*, *14*(12). <https://doi.org/10.1029/2022ms003074>